nature communications



Article

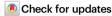
https://doi.org/10.1038/s41467-025-60505-x

Structural elucidation of a unique binding mode by an intact alphavirus human IgG molecule to a quaternary epitope

Received: 8 April 2024

Accepted: 24 May 2025

Published online: 19 August 2025



Abhishek Bandyopadhyay^{1,9}, Lauren E. Williamson $\textcircled{0}^{2,3,9}$, Devika Sirohi¹, Kevin Bailey⁴, Theron Gilliland Jr.⁵, Thomas Klose $\textcircled{0}^1$, Geeta Buda¹, Andrew Trivette², Chengqun Sun^{5,6}, Justin G. Julander⁴, William B. Klimstra^{5,6}, James E. Crowe Jr. $\textcircled{0}^{2,3,7,10} \boxtimes \&$ Richard J. Kuhn $\textcircled{0}^{1,8,10} \boxtimes$

Eastern equine encephalitis virus (EEEV) is a mosquito-transmitted alphavirus that can cause severe encephalitis in humans and horses with a high case fatality rate. There are no licensed EEEV vaccines or therapeutics for human use, warranting the need to better understand the human immune response against EEEV. Here we present a cryo-EM reconstruction of the chimeric virus, Sindbis (SINV)/EEEV, in complex with a potently neutralizing and efficacious intact human IgG1 antibody in a mouse model of infection and disease. This antibody requires bivalency to recognize a quaternary epitope on the E2 glycoprotein and cross-links two virus spikes across the icosahedral two-fold axis through a unique binding mode. Kinetic analysis of the binding interaction provides insights into this distinguishing feature. Mechanistically, the antibody inhibits viral entry into cells through blockade of receptor binding and early fusion events but does not block egress, thereby, exclusively targeting an epitope found on intact virions. The discovery of the quaternary epitope and unique binding mode recognized by this antibody together advance our understanding of the complexity of antibody-antigen interactions and can aid in vaccine design to elicit recognition of distinct epitopes of clinically relevant alphaviruses.

The humoral response to viral infections targets a wide range of epitopes on the virion, including quaternary epitopes¹⁻⁴. Antibodyantigen complexes help elucidate the structural basis for recognition of diverse epitopes by neutralizing antibodies. However, most of these studies used antibody Fab fragments instead of IgG, which limits our understanding of mechanism of action to monovalent antibody-

antigen interactions that may inaccurately describe the occupancy of bound sites on virion particles³⁻⁷. A more limited set of studies investigated intact neutralizing antibodies in complex with virion particles through structural analyses^{8,9}. To further our understanding of antibody-antigen interactions, we describe the structural and molecular analyses of a potently neutralizing human monoclonal antibody

¹Department of Biological Sciences, Purdue University, West Lafayette, IN 47907, USA. ²The Vanderbilt Center for Antibody Therapeutics, Vanderbilt University Medical Center, Nashville, TN 37232, USA. ³Department of Pediatrics, Vanderbilt University Medical Center, Nashville, TN 37232, USA. ⁴Institute for Antiviral Research, Utah State University, Logan, UT 84335, USA. ⁵The Center for Vaccine Research, University of Pittsburgh, Pittsburgh, PA 165261, USA. ⁶Department of Immunology, University of Pittsburgh, Pittsburgh, PA 165261, USA. ⁷Department of Pathology, Microbiology and Immunology, Vanderbilt University, Nashville, TN 37232, USA. ⁸Purdue Institute of Inflammation, Immunology and Infectious Disease, Purdue University, West Lafayette, IN 47907, USA. ⁹These authors contributed equally: Abhishek Bandyopadhyay, Lauren E. Williamson. ¹⁰These authors jointly supervised this work: James E. Crowe Jr., Richard J. Kuhn. ⊠e-mail: james.crowe@vumc.org; kuhnr@purdue.edu

(mAb) designated EEEV-373 as a bivalent IgG1 molecule in complex with the chimeric virus Sindbis (SINV)/Eastern equine encephalitis virus (EEEV).

The encephalitic alphaviruses are mosquito-transmitted viruses and include EEEV, Western (WEEV), and Venezuelan (VEEV) equine encephalitis viruses. EEEV is the most virulent amongst the encephalitic alphaviruses, with a reported human case fatality rate of ~30% and neurological sequelae in ~90% of survivors¹⁰⁻¹⁴. In the United States, on average 11 human cases of encephalitic disease caused by EEEV are reported each year (https://www.cdc.gov/easternequineencephalitis/). However, a spike in cases was observed in 2019, in which there were 38 reported human cases and 19 deaths across the United States due to EEEV. Although reported human case numbers decreased in the following years, 19 cases of EEEV neuroinvasive disease were reported in 2024, highlighting the concerns about the potential for larger future EEEV outbreaks. Unfortunately, there are no FDA-approved vaccines or antiviral treatments against EEEV available for human use. In addition, the encephalitic alphaviruses can be aerosolized for use as a potential bioweapon¹⁵. Given these significant concerns coupled with the lack of prevention or treatment options (vaccines or antiviral drugs) for humans, EEEV is classified as a NIAID Category B priority pathogen and an USDA/CDC Select Agent.

Alphaviruses are enveloped viruses with a positive-sense single-stranded -11.7 kb RNA genome that encodes both the non-structural and structural proteins $^{6,16-18}$. The alphavirus structural polyprotein encodes five to six structural proteins: capsid, E3, E2, 6K, E1, and TF (transframe). An alphavirus particle consists of a nucleocapsid core (NC) and glycoprotein layer. The NC consists of the capsid protein encapsulating the RNA genome with T=4 quasi-icosahedral symmetry and is comprised of 12 pentamers or 30 hexamers around the icosahedral five-fold (i5) or two-fold (i2) vertices, respectively. The NC is further encapsulated by the icosahedral glycoprotein layer consisting of the E2 and E1 single-pass transmembrane glycoproteins embedded in a host-derived lipid bilayer. The E2 and E1 glycoproteins form trimers of heterodimers arranged as 80 trimeric spikes on the surface of an alphavirus particle, with 20 spikes at the icosahedral three-fold (i3) and 60 spikes at the quasi-three-fold (q3) axes 6,17 .

The E2 glycoprotein forms the outermost layer of the viral particle and occludes most of the underlying E1 protein^{6,19}. The E2 glycoprotein engages cell-surface receptors and attachment factors, while the E1 glycoprotein lies tangential to the viral membrane and is responsible for endosomal viral fusion^{6,16,19-22}. The E2 glycoprotein consists of three immunoglobulin-like domains (A, B, and C), of which a "cleft" formed between domains A and B is involved in receptor interactions^{21–31}. In the past few years, several bona fide entry receptors were identified for alphaviruses through CRISPR/Cas9-based genetic screening approaches. Different receptors were identified for the arthritogenic (i.e., Mxra8^{23,24}) and encephalitic (i.e., VEEV: LDLRAD3^{25,26}) alphaviruses, which may contribute to differences in pathogenesis²¹. More recently, members of the low-density lipoprotein receptor (LDLR) family, very low-density lipoprotein receptor (VLDLR)^{28,29,31}, apolipoprotein E receptor 2 (ApoER2)²⁸, and LDLR³⁰ were identified as receptors for EEEV. Domain B also helps prevent premature exposure of the E1 fusion loop^{6,20,22,32,33}

Previous studies have described neutralizing anti-alphavirus antibodies that target different epitopes on the E2 glycoprotein (*i.e.*, domains A, B, and A/B) and can inhibit either cell attachment, receptor binding, viral fusion, virus egress, or a combination of these steps^{9,34–40}. On the other hand, several anti-E1 glycoprotein neutralizing antibodies have been described and appear to primarily block viral egress^{41,42}. Nevertheless, there are a limited number of studies describing antibodies that specifically target quaternary epitopes on alphavirus particles.

The structural analyses described here reveal a quaternary epitope on the E2 glycoprotein targeted by a human monoclonal antibody (mAb) designated EEEV-373. Potent efficacy of EEEV-373 was confirmed in cell culture and a mouse model of EEEV infection. This mAb distinctively binds by cross-linking two q3-spikes diagonally across the i2 axis governed by steric and distance constraints. Kinetic analysis of the antibody-antigen interaction provided mechanistic insights into the strict requirement for bivalent heterodimer binding. These data expand the scope of structure-guided immunogen design for clinically relevant alphaviruses. Furthermore, this study advances our growing knowledge on the complexity of antibody-antigen interactions for therapeutic antibody development.

Results

Identification and characterization of the potently neutralizing and efficacious human mAb EEEV-373

We isolated the human mAb EEEV-373 (IgG1, κ) from the B cells of an individual with prior documented natural EEEV infection using human B cell hybridoma cell technology. EEEV-373 was selected based on binding reactivity in ELISA to the chimeric virus Sindbis (SINV)/EEEV, EEEV virus-like particles (VLPs), and recombinant EEEV heterodimer (E2/E1) protein. The chimeric virus SINV/EEEV encodes the nonstructural proteins of SINV and the structural proteins of EEEV, which enables safe use of virus particles in biosafety level (BSL) -2 conditions⁴³.

To further characterize EEEV-373, we assessed the neutralization activity of hybridoma-cell-derived EEEV-373 IgG against wild-type EEEV (strain FL93-939) under BSL-3 conditions through a plaque reduction neutralization assay (Fig. 1A). EEEV-373 exhibited potent neutralization activity against EEEV, with a half-maximal inhibitory concentration (IC50) value of <37 pM (11 ng/mL). A minor residual fraction of non-neutralized virus (2%) was present at the highest concentration tested of 75 nM (22.5 μ g/mL), indicating incomplete neutralization of EEEV (Fig. 1B).

Next, we assessed the in vivo efficacy of EEEV-373 IgG against EEEV (strain FL93-939) infection in a subcutaneous (s.c.) treatment challenge model (Figs. 1C-E). In this model, EEEV was inoculated s.c. (10^{3.3} CCID₅₀) and antibody (IgG) was administered intraperitonially (i.p.) 24 h after virus inoculation. Mice were followed for a total of 21 days for survival, and viremia was assessed 3 days after virus inoculation using a plaque assay. In the EEEV-373 treatment group, 100% of the animals survived, compared to a 10% survival rate in the previously published negative control group treated with the recombinantly-derived dengue virus-specific mAb rDENV-2D22 (IgG1, λ)^{40,42,44} (Fig. 1C). The body weight of the animals corresponded with survival, in which body weight was relatively stable for the EEEV-373 treatment group compared to an observed loss in body weight for the rDENV-2D22 treatment group (Fig. 1D). We also observed a significant reduction in virus titer in the serum to the limit of detection of the assay for animals treated with EEEV-373, compared to those that received rDENV-2D22 (Fig. 1E).

EEEV-373 requires bivalent interactions for binding and neutralization of SINV/EEEV

To further characterize EEEV-373, we addressed whether bivalency is required for binding in ELISA (Fig. 2A). EEEV-373 as either bivalent IgG or F(ab')2 molecules bound to EEEV VLPs and recombinant EEEV E2/E1 protein. However, binding to recombinant monomeric EEEV E2 or E1 protein was not observed at the concentrations tested, which suggests EEEV-373 preferentially binds to a complex quaternary epitope. Maximal optical density signal was observed for binding to EEEV VLPs compared to EEEV E2/E1 protein, which suggested that there may be an avidity effect conferred by bivalent binding to virus particles. In contrast, EEEV-373 tested as monovalent Fab molecules did not appreciably bind to EEEV VLPs, recombinant EEEV E2/E1, E2, or E1 proteins at the concentrations tested. The lack of binding observed indicates EEEV-373 requires bivalent interactions for stable binding. To further

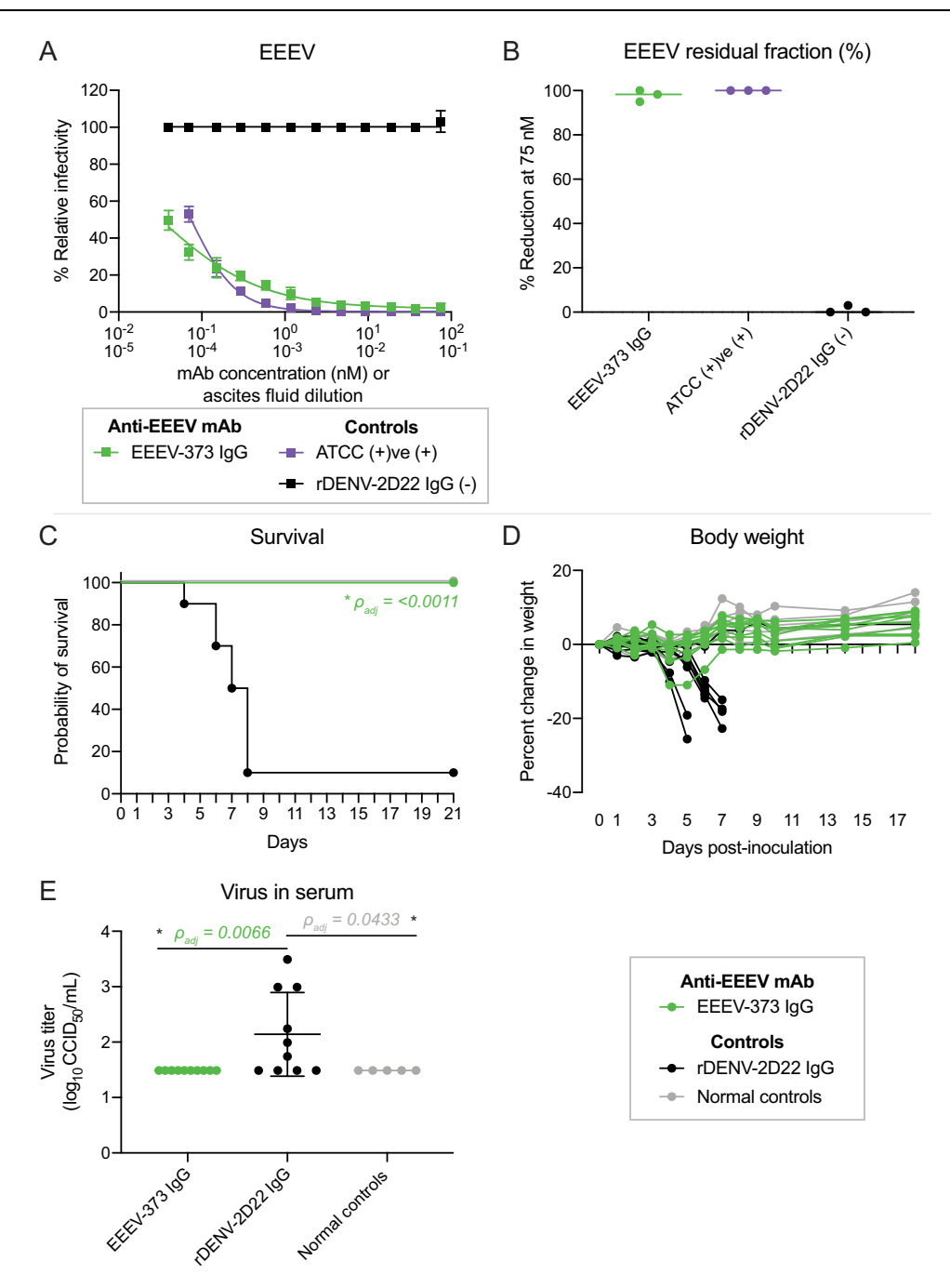


Fig. 1 | **EEEV-373 potently neutralizes and protects against wild-type EEEV. A** Neutralization curves of EEEV-373 (hybridoma-derived; green squares) as bivalent lgG1 molecules against wild-type EEEV strain FL93-939 in a plaque reduction neutralization assay. The previously published irrelevant isotype mAb (rDENV-2D22; black squares) or mouse anti-EEEV ascites fluid (ATCC (+)ve; purple squares) were included as negative or positive controls, respectively, for comparative purposes³⁹. Each curve displays mAb concentration (nM) or ascites fluid dilution on the *x*-axis and percent relative viral infectivity on the *y*-axis. Data represent mean \pm SD of technical triplicates of one biological replicate. **B** Percent of EEEV strain FL93-939 residual fraction (y-axis) present at the highest concentration tested (75 nM) of mAb (EEEV-373 [2%], rDENV-2D22 [99%], or ascites fluid [0%]). Data represent the median values of technical triplicates of one biological replicate. **C**-**E** EEEV (strain FL93-939; 10^{33} CCID₅₀) was inoculated subcutaneously (s.c.) into C57BL/6 mice. After 24 h, EEEV-373 (green) as bivalent lgG1 molecules was administered intraperitoneally (i.p.) at 10 mg/kg (200 μg/mouse; n = 10). The previously published negative control

treatment group, rDENV-2D22 (black; n = 10), or the mock-inoculated normal controls (grey; n = 5)^{40,42} also were included for comparative purposes. **C** EEEV-373 (green circles) or mock-inoculated normal control (grey circles) groups mediated 100% survival compared to the negative control mAb (rDENV-2D22; black circles) treatment group. Survival curves were compared using the log-rank test with Bonferroni multiple comparison correction (* ρ adj < 0.002). **D** Percent body weight change of each mouse from the EEEV-373 (green circles), rDENV-2D22 (black circles), or mock-inoculated normal control (grey circles) groups over the course of 18 days post-inoculation. **E** Serum was collected 3 days post-inoculation from each mouse of the treatment groups (EEEV-373 [green circles], rDENV-2D22 [black circles], or mock-inoculated normal controls [grey circles]) for quantification of virus titer (log₁₀ CCID₅₀/mL; y-axis) in an infectious cell culture assay. Data represent mean ± SD. The EEEV-373 and mock-inoculated normal control groups were compared to the rDENV-2D22 negative control treatment group using an ordinary oneway ANOVA with Dunnett's multiple comparisons test (* ρ < 0.05).

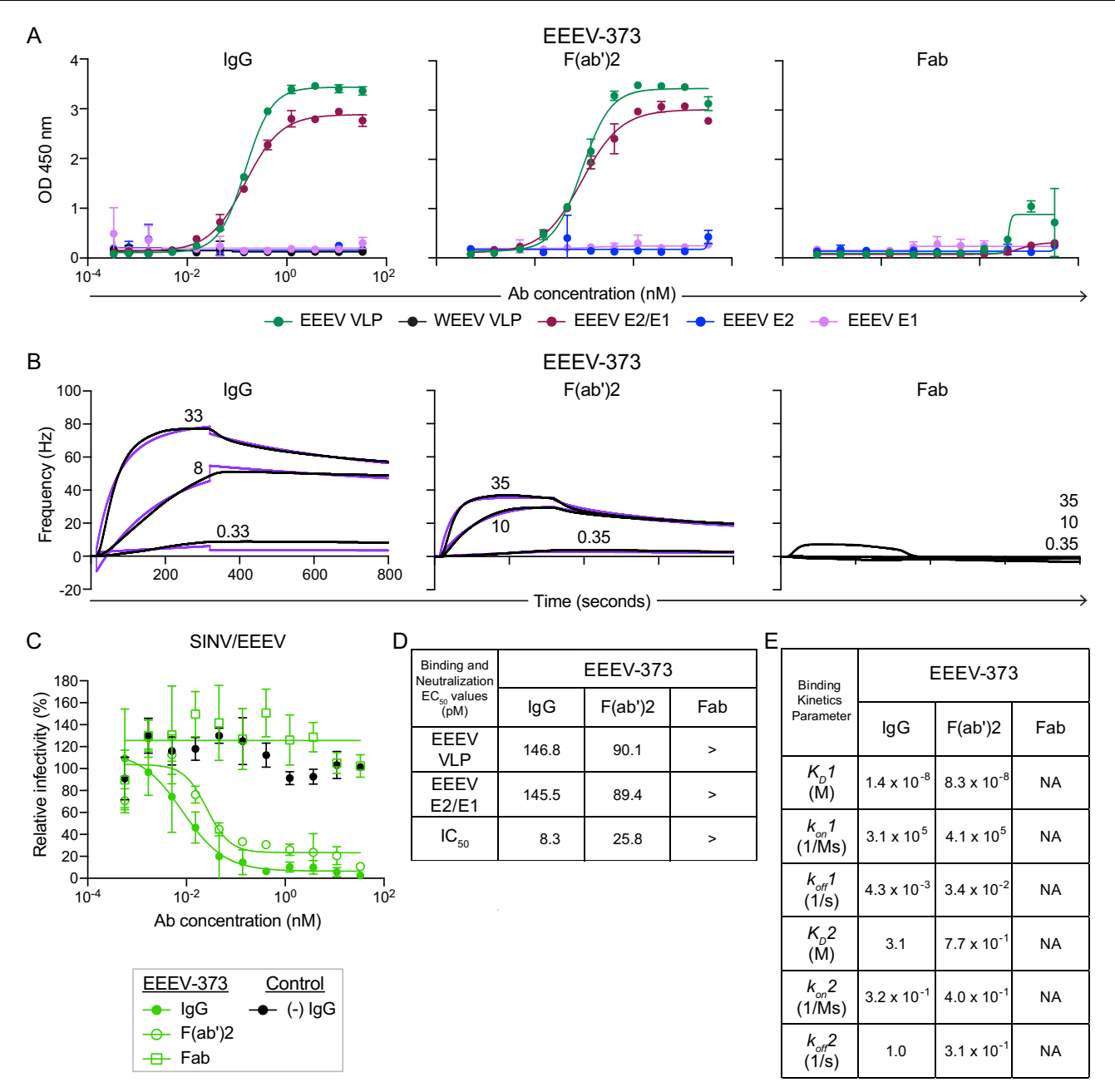


Fig. 2 | EEEV-373 binds and neutralizes EEEV in a bivalent manner.

A Representative binding curves of EEEV-373 as bivalent IgG1 (left), F(ab)2 (middle), or monovalent Fab (right) molecules to EEEV virus-like particles (VLPs; green circles), Western equine encephalitis virus (WEEV) VLPs (black circles), recombinant EEEV E2/E1 (maroon circles), monomeric E2 (blue circles) or E1 (light purple circles) protein. Each curve displays mAb concentration (nM) on the x-axis and optical density at 450 nm on the y-axis. Data represent mean \pm SD of technical triplicates and are representative of two independent experiments. **B** Representative binding kinetic curves (black lines) of EEEV-373 as bivalent IgG1 (left), F(ab)2 (middle), or monovalent Fab (right) molecules to EEEV VLPs using quartz crystal microbalance biosensors (Attana). EEEV VLPs were amine-coupled to chips and quenched with ethanolamine. EEEV-373 then was incubated with the chip for 300 s at the labeled concentration (0.33 to 35 nM) to determine the association rates (k_{ort}). Time (in seconds) is on the x-axis and

frequency (in hertz (Hz)) is on the y-axis. For analysis, a bivalent (IgG1 and F(ab')2) binding model was used, and corresponding fitted curves are shown by the purple lines. **C** Representative neutralization curves of EEEV-373 (green symbols) as bivalent IgG1 (closed circles), F(ab')2 (open circles), or monovalent Fab (open squares) molecules against the chimeric virus, SINV/EEEV. A negative control bivalent IgG1 mAb (black circles) also was included. Each curve displays mAb concentration (nM) on the x-axis and percent relative viral infectivity on the y-axis. Data represent mean \pm SD of technical triplicates and are representative of two independent experiments. **D** Summary table of the half-maximal effective (EC₅₀) concentration values for binding of EEEV-373 as bivalent IgG1 (left column), F(ab')2 (middle column), or monovalent Fab (right column) molecules to EEEV VLPs or recombinant EEEV E2/E1 protein, and half-maximal inhibitory (IC₅₀) values for neutralization activity against SINV/EEEV. **E** Summary table of kinetic analyses (K_{D} , k_{on} , k_{off}) for EEEV-373 as bivalent IgG1 (left column), F(ab')2 (middle column) molecules.

assess the dependence of EEEV-373 on bivalency, we tested the neutralization potency of EEEV-373 against SINV/EEEV (Fig. 2C). Consistent with the binding profile of EEEV-373, the IgG and F(ab')2 formats of the antibody neutralized SINV/EEEV with similar potencies, although a -3-fold reduction in IC₅₀ value was observed for the F(ab')2 format

(Fig. 2D). In contrast, EEEV-373 Fab molecules failed to neutralize SINV/EEEV.

We next assessed the binding kinetics of EEEV-373 IgG, F(ab')2, or Fab molecules with EEEV VLPs using quartz crystal microbalance biosensors (Figs. 2B, E). In this assay, we also observed binding of EEEV-

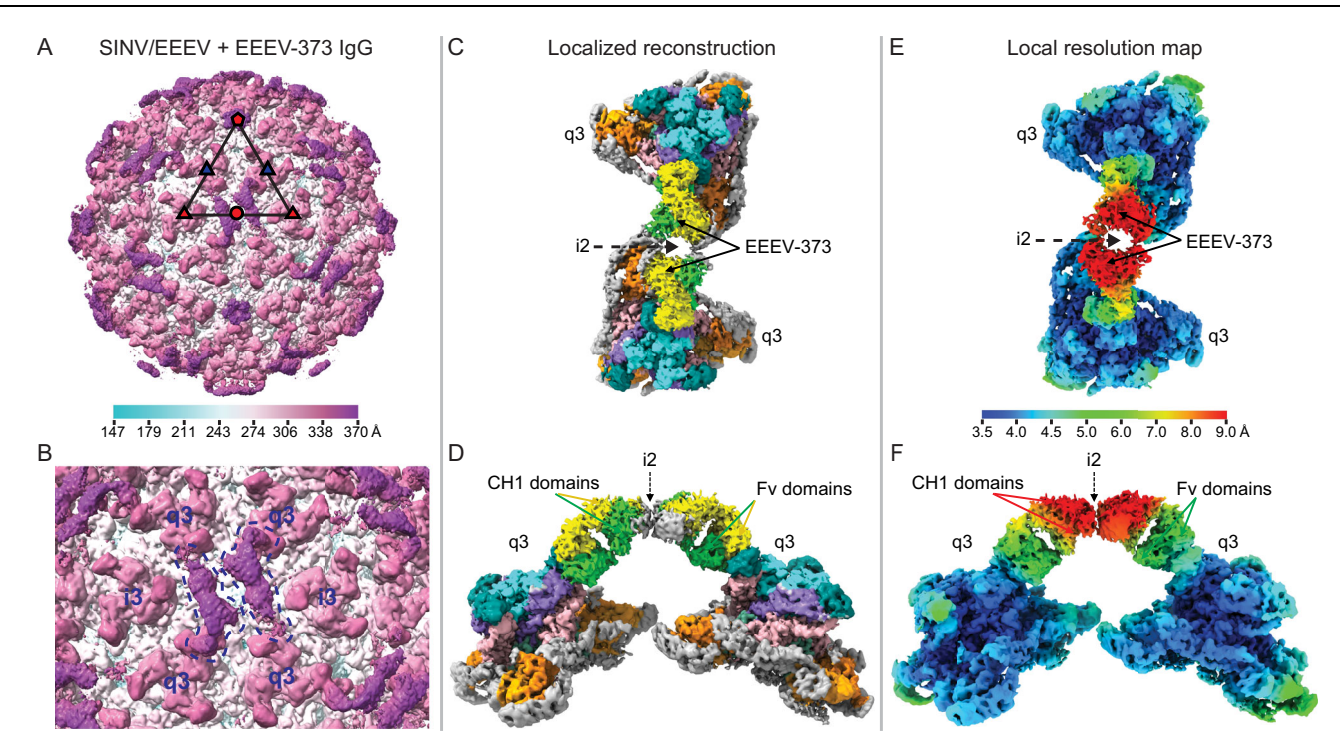


Fig. 3 | **Cryo-EM reconstruction of SINV/EEEV in complex with a potently neutralizing intact IgG. A** Cryo-EM reconstruction of SINV/EEEV particles in complex with EEEV-373 IgG was determined by single particle averaging with icosahedral symmetry to 4.6 Å resolution. The black triangle represents the asymmetric unit, with the symmetry axes depicted by the red pentagon (5-fold axis), triangle (3-fold axis), and circle (2-fold [i2] axis) symbols. The quasi-three-fold (q3) spikes are represented by the blue triangles. The scale bar (in Å) represents the radial distance from the center of the virus. B A close-up view of the i2 axis displays a single EEEV-373 IgG molecule diagonally spanning across the axis to connect two q3 spikes. The q3 and icosahedral three-fold (i3) spikes are labeled in dark blue text accordingly. In comparison to the SINV/EEEV particle density, the density of the IgG molecule is relatively weak, and to help elucidate the complex, the two arms of the IgG molecule are indicated by the dark blue

dotted lines. **C**, **D** Localized reconstruction, focused classification, and refinement with C1 symmetry of the two q3 spikes cross-linked by the EEEV-373 lgG molecule were performed to improve the resolution of the reconstruction. A top (**C**) or side (**D**) view of the improved reconstruction from the i2 axis perspective are illustrated. The q3 spikes, constant and variable domains of EEEV-373 are indicated accordingly. The map is colored according to the coloring of the fitted model in ChimeraX. The grey regions fall slightly outside of the fitted model, while the relative protein domains of E1 (domain I: orange, domain II: light pink, domain III: light orange), E2 (domain A: cyan, domain B: teal, domain C: aqua, β -ribbon connector: purple), EEEV-373 heavy chain (green) and light chain (yellow) are colored accordingly. **E**, **F** Local resolution map of the volume as shown in **C** and **D**. **E**, **F** correspond to the viewing directions in **C** and **D**, respectively. The scale bar (in Å) represents the resolution gradient.

373 to EEEV VLPs in a bivalent manner. For binding of EEEV-373 IgG or F(ab')2 molecules to EEEV VLPs, we observed a biphasic association pattern in which there was a fast initial binding interaction (10⁵ Ms⁻¹) followed by a slower second phase interaction ($10^{-1} \,\mathrm{Ms^{-1}}$). The K_D , k_{on} , and k_{off} values for both IgG and F(ab')2 molecules are similar (Fig. 2E), suggesting that the Fc region of the antibody does not play a major role in the binding interaction. Further supporting this, we also observed a similar association profile for binding of bivalent EEEV-373 IgG and F(ab')2 molecules to EEEV VLPs using biolayer interferometry (Fig. S1). In contrast to bivalent molecules, a weak association was observed for Fab molecule binding to EEEV VLPs. This weak association corresponds with the variable detectable signal observed at the highest concentrations of Fab molecules for binding to EEEV VLPs as tested via ELISA (Fig. 2A). However, in comparison, binding of EEEV-373 Fab molecules to EEEV VLPs was not detected using biolayer interferometry (Fig. S1). In this case, the interaction was comparable to that of a negative control IgG. A potential explanation for the observed kinetic behavior of Fab molecules may be the inability to form stable antibody-antigen complexes. The biphasic association pattern of bivalent IgG or F(ab')2 molecules indicates that complex formation involves more than one step. The initial interaction may be energetically weak, as reflected by the poor binding of Fab molecules. The avidity effects of bivalent molecules may compensate for this weak interaction by engagement of two binding sites, shifting the equilibrium towards formation of a high affinity complex.

Cryo-EM reconstruction of EEEV-373 as an IgG1 molecule in complex with SINV/EEEV particles

To elucidate the structural determinants of bivalent binding and neutralization, we obtained a three-dimensional cryo-EM reconstruction of SINV/EEEV particles in complex with EEEV-373 as an IgG1 molecule. The reconstruction was determined to ~4.6 Å with imposed icosahedral symmetry (Fig. 3A). Although the density of the IgG was weak compared to the glycoprotein densities, a single EEEV-373 IgG molecule connecting two q3 spikes diagonally across the i2 axis was visible (Figs. 3A, B). An even weaker and broken density around the i5 axis was also observed. This density likely reflects low IgG occupancy around the i5 axis, suggesting that the predominant mode of binding cross-links the q3 spikes across the i2 axis (Fig. S6D). To improve the density of the antibody and fit atomic models, localized reconstruction combined with focused classification and refinement of the two q3 spikes bound to EEEV-373 were performed, providing a global resolution estimate of ~3.8 Å (Figs. 3C, D, and S7). The overall density of the EEEV-373 IgG molecule at the i2 axis improved, with the local resolution map estimation showing the variable domains resolved significantly better than the constant domains (Figs. 3E, F). The local resolution map estimates the resolution of the variable domains to be ~5 Å, whereas that of the constant domains was greater than ~9 Å. We did not observe any density for the hinge or Fc region of the IgG molecule.

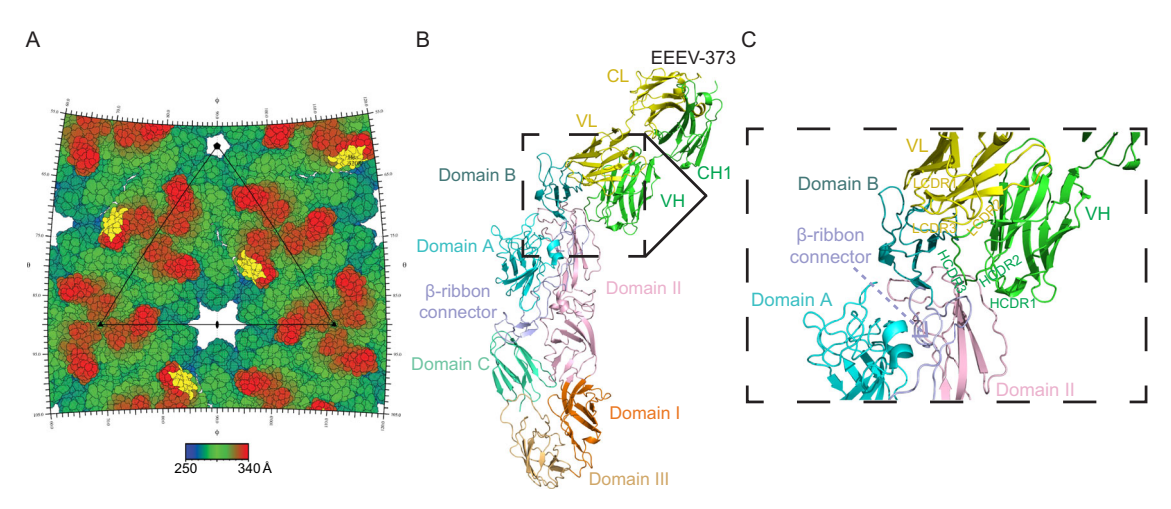


Fig. 4 | **EEEV-373** epitope binding footprint on SINV/EEEV particles. A RIVEM (Radial Interpretation of Viral Electron Density Maps) representation of the EEEV-373 IgG binding epitope on the viral surface. Residues within 6 Å of the complementarity-determining regions (CDRs) of EEEV-373 IgG are colored yellow and constitute the epitope binding footprint on the viral surface. The scale bar represents the radial distance in Å from the center of the virus. **B** Cartoon representation of one arm of the EEEV-373 IgG molecule in complex with a unit of the SINV/EEEV E2/E1 heterodimer. The different protein domains of E1 (domain I: orange, domain II: light pink, domain III: tan), E2 (domain A: cyan, domain B: teal,

domain C: aqua, β -ribbon connector: light purple), EEEV-373 heavy chain (green; VH: variable domain, CH1: constant domain), and EEEV-373 light chain (yellow; VL: variable domain, CL: constant domain) are labeled accordingly. **C** A close-up view of the interface between EEEV-373 and the SINV/EEEV E2/E1 heterodimer. The heavy (green) or light (yellow) chain CDRs 1-3 are indicated as HCDR1, HCDR2, HCDR3 or LCDR1, LCDR2, LCDR3, respectively. The E2 protein domain A (cyan), domain B (teal), β -ribbon connector (light purple), and E1 protein domain II (light pink) are labeled accordingly.

Identification of a quaternary epitope targeted by EEEV-373 on the E2/E1 glycoproteins

From the cryo-EM reconstruction, we observed that EEEV-373 primarily binds the E2 glycoprotein of SINV/EEEV particles (Fig. 4 and S2). The total area buried by EEEV-373 on the E2/E1 glycoprotein is 750.5 $Å^2$, with the heavy or light chain burying $402 \, \text{Å}^2$ or $348.5 \, \text{Å}^2$, respectively. To determine the binding footprint of EEEV-373 on the E2/E1 glycoproteins, residues within 6 Å of the backbones of the fitted atomic model were identified. The binding footprint of EEEV-373 constitutes several residues on the E2 glycoprotein and one residue (K61) within domain II of the E1 glycoprotein. Except for K61, all remaining residues are not conserved amongst other alphaviruses (Fig. S4). This finding supports the specificity of EEEV-373 to EEEV, as we did not observe detectable binding to Western equine encephalitis virus (WEEV) VLPs by ELISA at the concentrations tested (Fig. 2A). Based on the binding footprint, the light chain of EEEV-373 binds surface exposed residues within domain B of the E2 glycoprotein, and the heavy chain binds the E2 β-ribbon connector and residue K61 of the E1 glycoprotein (Figs. 4C, 5, and S2). The heavy chain complementarity-determining regions (CDRs) clamp onto the β-ribbon connector (residues 230 to 248), which is spatially adjacent to domain B and includes the 'arch 2' region²² (Figs. 4, 5, and S2). The β-ribbon connector essentially is a long linker connecting domains A to B and B to C, with little secondary structure. Natively, the 'arch 2' region of the β-ribbon connector forms a narrow cleft-like structure and makes significant interactions with the underlying E1 protein (Figs. 5A, B). Thus, it is conceivable that in the absence of the E1 protein, the β-ribbon connector might be flexible, and as a result the cleft of the 'arch 2' region would become unstable. EEEV-373 binding shows that CDRH1 and CDRH2 clamp onto the 'arch 2' region (Figs. 5C, D), with CDRH3 inserting into the cleft (Figs. 5E, F). The heavy chain interaction with residue K61 of the E1 glycoprotein is largely due to its long side chain, as no other residue in the vicinity of K61 contributes to the binding footprint of EEEV-373. The interactions observed for the heavy chain CDRs with the E2 glycoprotein, suggest that EEEV-373 binding critically depends on the conformational nature of the heterodimer through the interaction of the E2 β-ribbon connector with the E1 protein, consistent with the ELISA binding data (Fig. 2).

To further determine the most functionally relevant interactions in the binding footprint of EEEV-373, we assessed the ability for SINV/ EEEV to escape neutralization under antibody selective pressure. In the presence of EEEV-373 at saturating antibody concentrations, we identified escape mutant viruses with a E147K mutation in the E2 protein (Fig. S3). This residue corresponds to the β -ribbon connector outside of the EEEV-373 binding footprint as determined by cryo-EM (Fig. S4). Given the potential flexibility and conformational dependence of the β -ribbon connector for binding, the E147K mutation may allosterically alter the conformation of the epitope, ablating the neutralization capabilities of EEEV-373.

EEEV-373 cross-links viral q3 spikes using a preferred binding mode

In the cryo-EM reconstruction of EEEV-373 IgG in complex with SINV/ EEEV particles, we predominantly observe one binding orientation with the IgG molecule connecting two q3-spikes across the i2 axis (q3.1-q3.3). Based on previous studies, the distance between the CH1 domains (Cys216 [Kabat numbering]) of the arms of an IgG molecule is ~50 Å, allowing for intra-virion cross-linking of icosahedral viruses^{40,45}. However, since the resolution of the constant domains is ~9 Å in our reconstruction, we are unable to accurately determine the position of Cys216, which corresponds to Cys228 for EEEV-373. Instead, we used the last residue on strand G of the CH1 domain⁴⁶ (Lys222 in EEEV-373) to determine the distances more accurately between the two arms of the EEEV-373. There are 12 residues that act as a long flexible linker between the last residue on strand G and the cysteine residue that forms the first disulfide bond in the hinge region (Cys222 [Kabat numbering]). The length of this flexible segment when fully stretched is ~48 Å. Thus, the distance criteria for the arms of an IgG molecule ranges from ~50 to 100 Å.

In the preferred q3.1–q3.3 binding mode of EEEV-373, the distance between Lys222 of the CH1 domains is -42.5 Å (Fig. 6A), which is well within the range (-50–100 Å) that allows for an IgG molecule to bind two epitopes^{40,45}. Since the i2 axis of alphaviruses is quasi 6-fold, there are five additional ways EEEV-373 could cross-link viral spikes across the i2 axis (Fig. 6B). To investigate why we observed this preferential q3.1–q3.3 mode of binding, we superimposed the atomic

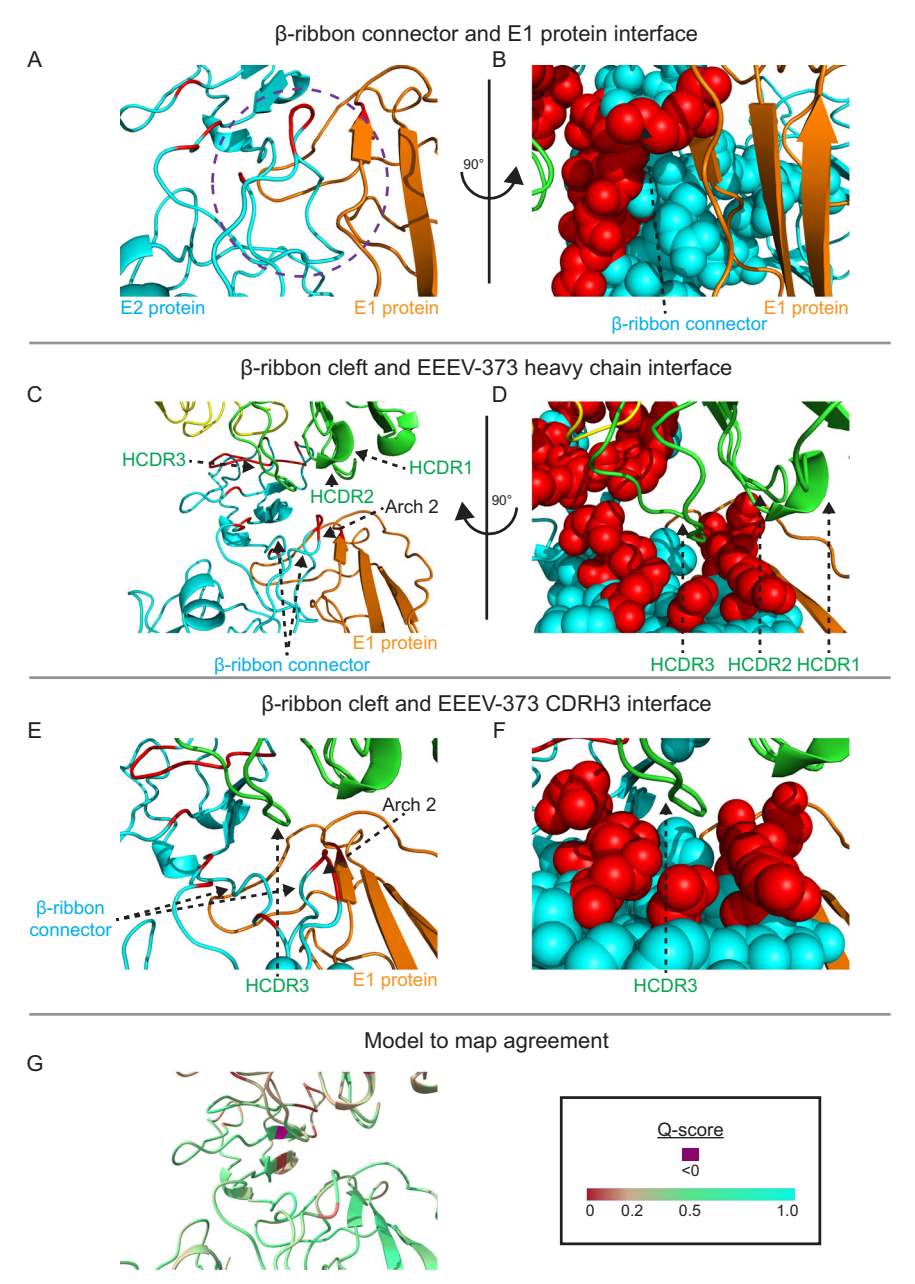


Fig. 5 | **EEEV-373** binds a conformational epitope on the SINV/EEEV E2 protein. **A** A close-up view of the E2 protein β -ribbon connector (cyan) and the E1 protein domain II (orange) interface, further highlighted by the dotted purple circle. The residues comprising the binding footprint of EEEV-373 are colored red. **B** A side view (rotated -90°) of the E2/E1 interface is shown to highlight the significant interaction of the underlying E1 protein (orange) for the proper conformation and stabilization of the E2 protein β -ribbon connector (cyan). Residues involved in this interaction are indicated by the cyan or red spheres. The red spheres indicate the E2 residues that constitute the EEEV-373 epitope binding footprint. A detailed cartoon representation view (**C**) and a close-up, side view (rotated -90°; **D**) of the interactions

between the heavy chain complementarity-determining region loops (HCDR1, HCDR2, and HCDR3) of EEEV-373 (green) and the 'arch 2' cleft of the E2 protein β -ribbon connector (cyan). Specific view of the heavy chain CDR3 loop (HCDR3) of EEEV-373 (green) inserting within the 'arch 2' cleft of the E2 protein β -ribbon connector (cyan) as shown by the cartoon (**E**) or sphere (**F**) representations. The E2 protein β -ribbon connector residues that form the epitope binding footprint of EEEV-373 are indicated by the red spheres. Additional residues on the E2 protein within the immediate vicinity of the footprint are indicated by the cyan spheres. **G** The quality of the model fit to the map in the epitope-paratope region is coloured according to the Q-score. The corresponding color key is shown on the right.

model of the E2 glycoprotein bound to an EEEV-373 Fab arm from the q3.1 spike onto the i3 (i3.1 and i3.2) and q3.4 spikes. This fitting shows that in the i3.1–i3.2 binding mode, the distance between Lys222 of the CH1 domains of EEEV-373 is -64 Å (Fig. 6C), which may be too distant or require stretching for both arms of the EEEV-373 IgG molecule to simultaneously bind. Additional binding modes lead to severe clashes of the CL domains, such as in the case of cross-linking adjacent i3.1–q3.1 spikes (Fig. 6D) or between the q3.3–q3.4 spikes (-44.2 Å; Fig. 6G). These clashes probably restrain binding of the IgG

molecule to the preferred q3.1–q3.3 orientation. Interestingly, the q3.1–q3.4 binding mode satisfies both the distance criteria (-41 Å) and the fitted models do not appear to clash (Fig. 6E). However, the poor resolutions of the CL and the CH1 domains, as estimated from the local resolution maps, suggest these regions are highly flexible. Due to flexibility of the elbow region, movement of the constant domains perpendicular to the pseudo-2-fold axis of the Fab (between the heavy and light chains) can occur³6. Therefore, movement of the constant domains could lead to clashes between the two arms of the

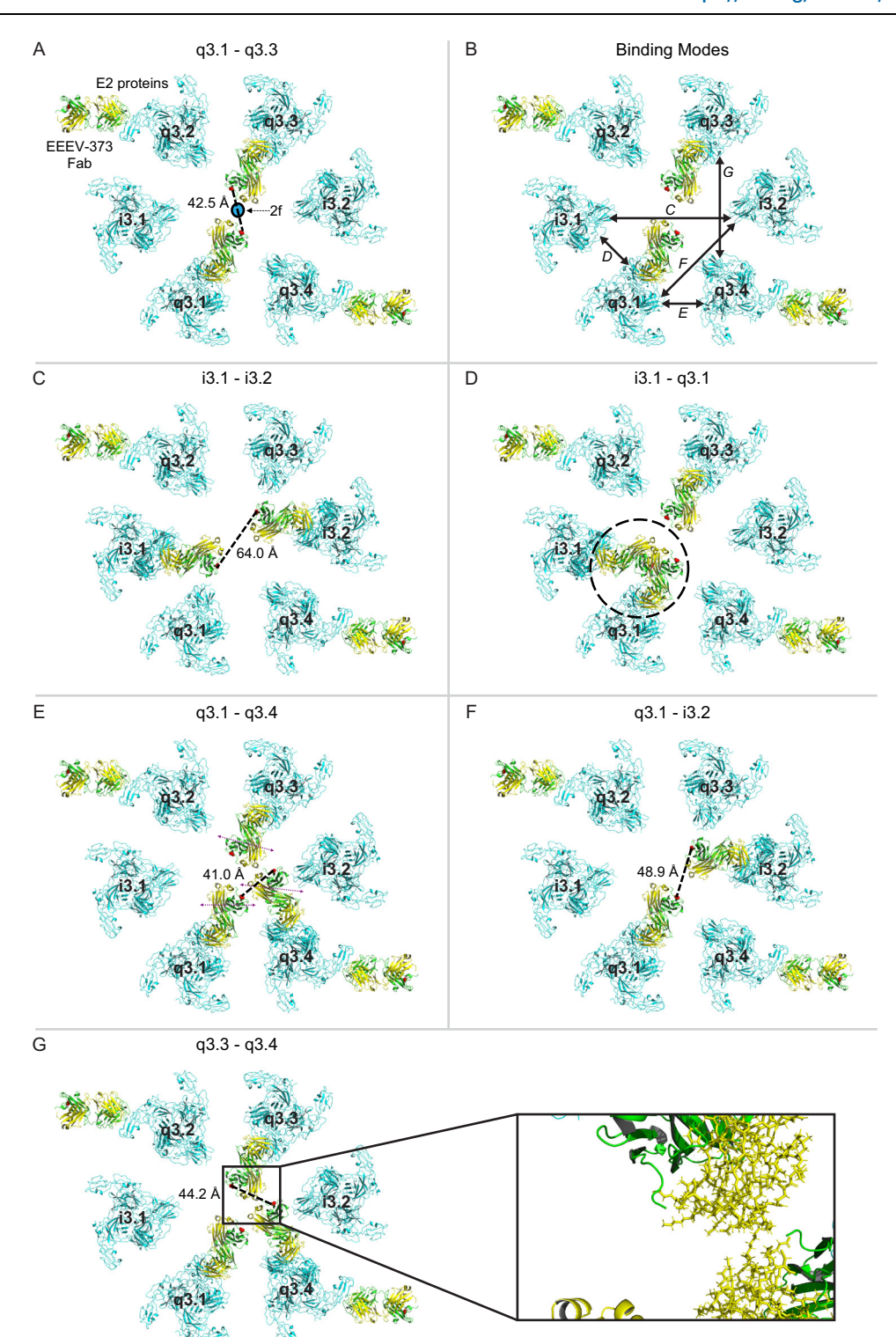


Fig. 6 | **Potential binding modes of EEEV-373 IgG at the icosahedral 2-fold axis of SINV/EEEV particles.** A Preferred binding mode orientation of EEEV-373 IgG across the icosahedral 2-fold (i2) axis (q3.1-q3.3). A cartoon representation of the fitted atomic models of the E2 protein (cyan) and EEEV-373 IgG (heavy chain: green, light chain: yellow) at the i2 axis (blue circle) is shown. The E1 protein is omitted for clarity. The four q3 spikes (q3.1-q3.4) and the two i3 spikes (i3.1-i3.2) are labeled in bolded text accordingly. The distance (in Å) between the $C\alpha$ atoms of the last residue (Lys222; red spheres) on strain G of the constant domains (CH1) of the two Fab arms of EEEV-373 (42.5 Å) is indicated by the dotted line. **B** In addition to the observed binding mode, there are five alternative ways (**C**–**G**) EEEV-373 could crosslink viral spikes across the i2 axis as depicted. The distance (in Å) between the $C\alpha$ atoms of the last residue (Lys222; red spheres) on strain G of the constant domains

(CHI) of the two Fab arms of EEEV-373 are indicated by the dotted lines (\mathbf{C} [i3.1-i3.2]: 64.0 Å; \mathbf{E} [q3.1-q3.4]: 41.0 Å; \mathbf{F} [q3.1-i3.2]: 48.9 Å; \mathbf{G} [q3.3-q3.4]: 44.2 Å). For the i3.1-q3.1 (\mathbf{D}) or q3.3-q3.4 (\mathbf{G}) binding modes, steric clashes are observed between the light chain constant domains of EEEV-373 (yellow) as indicated by the black dotted circle (\mathbf{D}) or the black box (\mathbf{G}). \mathbf{E} For the q3.1-q3.4 binding mode, movement of the constant domains as indicated by the purple arrows may lead to steric clashes. \mathbf{F} For the q3.1-i3.2 binding mode, EEEV-373 may also bind in this orientation. However, a 60° rotation of one Fab arm with respect to the other Fab arm may reduce the likelihood of binding. The distance and steric hindrance constraints observed in \mathbf{C} - \mathbf{G} likely contribute to the observation of EEEV-373 in the preferred binding mode orientation (\mathbf{A}) with binding of the two Fab arms to the q3.1 and q3.3 spikes across the i2 axis.

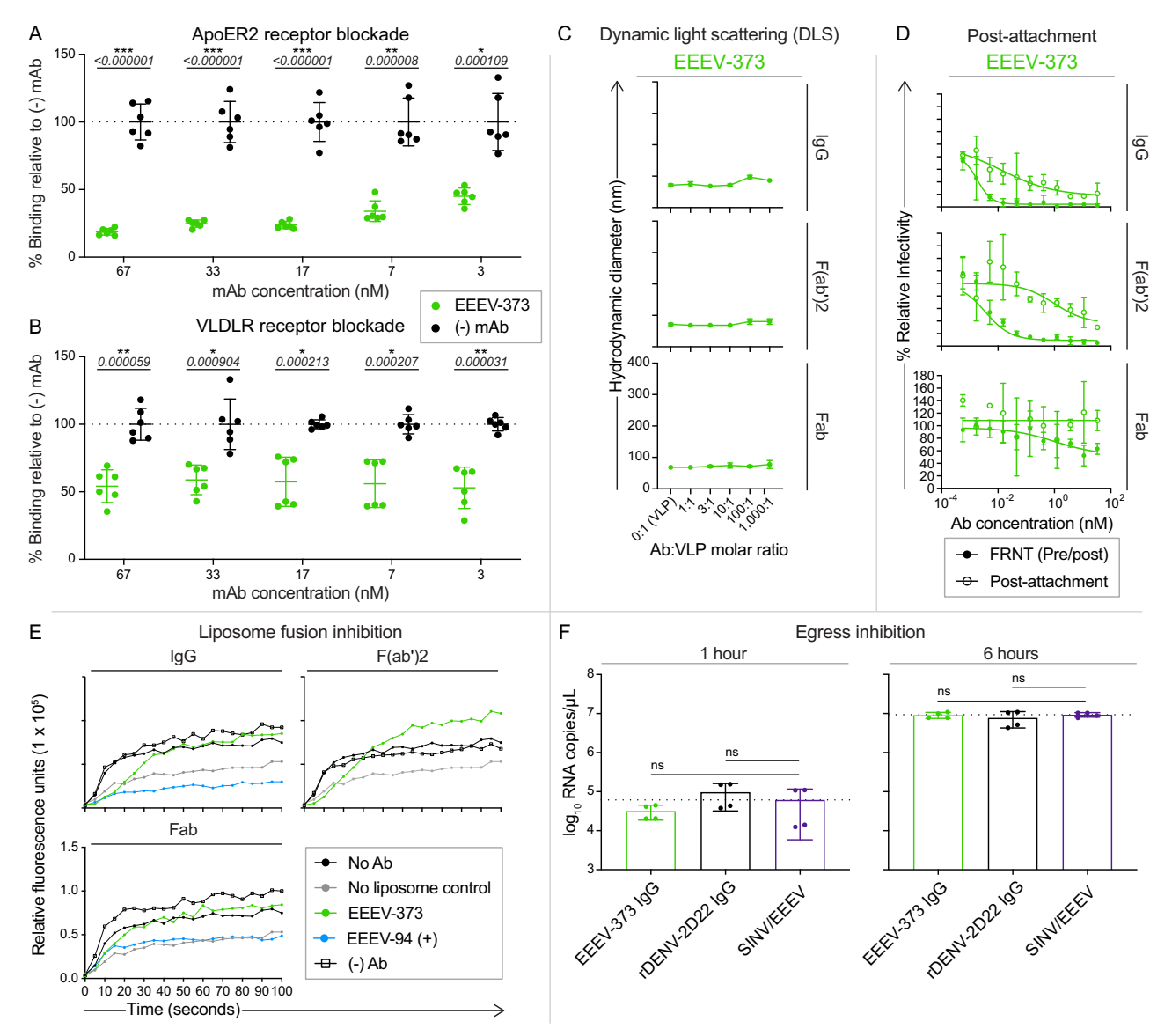


Fig. 7 | EEEV-373 inhibits SINV/EEEV entry through receptor blockade and inhibition of early fusion events. Competition-binding ELISA to assess the ability of bivalent EEEV-373 (green) or isotype-matched control (black) IgG1 molecules to block ApoER2 (A) or VLDLR (B) protein receptors from binding to EEEV VLPs at the concentrations indicated (67 to 3 nM; x-axis). The average optical density at 450 nm of the isotype-matched control mAb at each concentration was calculated and used to normalize the percent binding of EEEV-373 to EEEV VLPs (y-axis). Data represent mean ± SD of technical triplicates of two independent experiments. Data were analyzed at the specified concentrations using multiple unpaired t-tests (*** ρ < 0.000001, ** ρ < 0.0001, * ρ < 0.001). The exact ρ values are noted for each comparison. C Dynamic light scattering (DLS) of EEEV-373 (green) as bivalent IgG1 (top), F(ab')2 (middle), or monovalent Fab (bottom) molecules at different Ab:VLP molar ratios (xaxis). The peak hydrodynamic diameter (nm) is shown on the y-axis. Data represent mean ± SD of technical duplicates and are representative of two independent experiments. D Representative neutralization curves of EEEV-373 (green) as bivalent IgG1 (top), F(ab')2 (middle), or monovalent Fab (bottom) molecules assessed by a post-attachment assay (open circles) or focus reduction neutralization test (FRNT; closed circles). Ab concentration (nM) is on the x-axis and percent relative infectivity

is shown on the y-axis. Data represent mean ± SD of technical duplicates and are representative of two independent experiments. E Liposomal fusion assay of DiDlabeled SINV/EEEV particles incubated with liposomes in the presence of EEEV-373 (closed green circles), EEEV-94 (closed cyan circles; positive control), or an isotypematched control (open black squares; negative control) as bivalent IgG1 (top left), F(ab')2 (top right), or monovalent Fab (bottom left) molecules. Assay controls in which no antibody (closed black circles) or liposomes (closed grey circles) were also included. Data are representative of two independent experiments. F An egress inhibition assay was performed to determine the relative RNA copies/µL present in supernatant harvested at either 1 h (left) or 6 h (right) after addition of EEEV-373 (green) or the previously published⁴⁰ irrelevant isotype control mAb, rDENV-2D22 (black), as bivalent IgG1 molecules. RNA copies/µL were determined using a standard curve with quantitative EEEV RNA (ATCC). SINV/EEEV RNA levels were compared to the previously published 40 SINV/EEEV only control group (purple) using an ordinary one-way ANOVA with Dunnett's multiple comparisons test (ns = not significant). The previously published negative control mAb, rDENV-2D22, and SINV/EEEV only control groups were included for comparative purposes⁴⁰. Data represent mean ± SD of technical quadruplicates and are representative of two independent experiments.

IgG in the q3.1–q3.4 binding mode. In the observed q3.1–q3.3 binding mode, this movement does not lead to clashes between the two arms of the IgG molecule. The last binding mode (q3.1–i3.2) satisfies the distance criteria (-48.9 Å) and does not sterically clash (Fig. 6F), yet we do not observe this mode of binding in the structure. The only difference between q3.1–q3.3 and q3.1–i3.2 binding modes is the

rotation of one Fab arm about 60° with respect to the other arm, which may cause tension on the IgG molecule. However, it is not obvious from the structure as to why this mode of binding is not observed. Together, these observations suggest stringent criteria (*i.e.*, distance and angle of binding) are required for EEEV-373 IgG to bind and form intra-virion spike cross-links.

EEEV-373 does not aggregate EEEV VLPs by formation of intra-virion spike cross-links

To functionality validate the observed structural basis of neutralization by EEEV-373, we aimed to elucidate the molecular mechanism of action of EEEV-373 against EEEV. Based on the cryo-EM reconstruction, the observed binding orientation of EEEV-373 displays formation of intra-virion spike cross-links by the IgG molecule. To further corroborate this, we tested the ability of EEEV-373 to aggregate VLPs using dynamic light scattering (DLS) (Fig. 7C). The hydrodynamic diameter of antibody-antigen complexes at different molar ratios can be estimated using DLS. The diameter of the VLP alone was ~70 nm, which is close to the expected value for an alphavirus particle¹⁶. At any of the molar ratios tested, EEEV-373 as IgG or F(ab')2 molecules minimally aggregated VLPs. This finding strongly supports the formation of intravirion spike cross-links by EEEV-373 binding to two q3 spikes across the i2 axis. At very high molar ratios (>1:100 IgG:VLP), a slight increase in hydrodynamic diameter to ~100 nm is observed. This finding may result from partial binding of EEEV-373 to additional exposed epitopes present on two neighboring virus particles (inter-virion spike crosslinks) following complete occupancy of the preferred binding orientation within the same virus particle (intra-virion spike cross-links). Binding to these exposed epitopes may account for the observed weak density around the i5 axis in the icosahedral reconstruction. As expected, we did not detect aggregation of EEEV VLPs by EEEV-373 Fab molecules.

EEEV-373 blocks receptor binding to EEEV VLPs

Members of the low-density lipoprotein receptor (LDLR) family, apolipoprotein E receptor 2 (ApoER2)²⁸ and very low-density lipoprotein receptor (VLDLR)^{28,29,31}, were recently identified as receptors for EEEV. To assess the ability of EEEV-373 to block receptor interactions, we performed a competition-binding ELISA with ApoER2 and VLDLR (Figs. 7A, B). In this assay, EEEV VLPs were incubated with EEEV-373 or a negative control mAb as IgG1 molecules. ApoER2 or VLDLR then was added to detect whether receptor binding can occur in the presence of mAb. Based on the results, EEEV-373 blocked ~80% or ~50% of the interactions with ApoER2 or VLDLR, respectively, compared to the negative control mAb. Recently, the VLDLR binding footprint on the E2 glycoprotein of EEEV was identified^{29,31}. The E2 residues making the most significant interactions with VLDLR (H155, K156, and R157) are on the 'central arch' region of the β-ribbon connector, which is adjacent to domain A. This region is distinct from the EEEV-373 binding site, which is on 'arch 2' of the β -ribbon connector. Therefore, it is likely that the partial inhibition of VLDLR binding to EEEV by EEEV-373 is through steric blockade of cognate receptor binding or by allosteric modulation of the β-ribbon connector. The receptor binding site for ApoER2 on EEEV is not known yet. However, the results observed suggests EEEV-373 may bind within or nearby the receptor binding site to block or sterically hinder ApoER2 binding (Fig. S4). As EEEV-373 binds in a preferential manner across the i2 axis, incomplete occupancy of exposed receptor binding sites may occur. Under saturating conditions, 60 out of 80 trimeric spikes are stably occupied with EEEV-373 IgG per virion. For the occupied 60 q3 spikes, only a third of the E2 glycoproteins are bound by IgG, exposing the remaining E2 glycoproteins for receptor binding. This mechanism likely accounts for the observed residual binding of these receptors to EEEV VLPs in the presence of saturating concentrations of EEEV-373.

EEEV-373 partially inhibits SINV/EEEV after virus attachment to cells

We next tested the ability of EEEV-373 to neutralize SINV/EEEV after initial attachment to a Vero cell monolayer using a post-attachment inhibition assay (Fig. 7D), as previously described in refs. 39,40. In this assay, Vero cells were incubated with SINV/EEEV particles at 4 °C to allow for virus attachment. EEEV-373 then was added, and the cells

were shifted to 37 °C to enable virus entry. In comparison to a standard focus reduction neutralization assay (FRNT, Fig. 7D), EEEV-373 still neutralized SINV/EEEV as IgG or F(ab')2 molecules after virus attachment to Vero cell monolayer cultures. However, a reduced potency in neutralization was observed (-8- to >200-fold shift in IC $_{50}$ values for IgG or F(ab')2, respectively). This finding may be due to the inaccessibility of all epitopes through interactions between virus particles and cellular receptor or attachment factors on cells, leading to incomplete neutralization. Thus, EEEV-373 may partially neutralize through receptor blocking as previously described and is unable to neutralize as efficiently once the virus has already interacted with cells. Consistent with previous data (Fig. 2C), EEEV-373 Fab molecules did not neutralize SINV/EEEV.

EEEV-373 inhibits initial low-pH-induced fusion of SINV/EEEV with liposomes

We next assessed whether EEEV-373 inhibits low-pH-induced fusion of SINV/EEEV with liposomes as previously described in ref. 40. This assay serves as a surrogate for virus fusion with the endosomal membrane during alphaviral infection of cells by measuring the dequenching of DiD (1,1'-dioctadecyl-3,3,3',3'-tetramethylindodicarbocyanine, 4-chlorobenz enesulfonate salt)-labeled SINV/EEEV particles. In this assay, DiDlabeled SINV/EEEV particles were incubated with an excess of unlabeled liposomes (200 nm in size) and membrane fusion was triggered by acidification with a low-pH buffer (final pH ~5.2). Viral fusion was measured by dilution of DiD within the liposomal membrane, and a subsequent increase in fluorescence intensity over time. Inhibition of SINV/EEEV fusion was measured by the reduction of DiD fluorescence dequenching. Pre-incubation of DiD-labeled SINV/EEEV particles with EEEV-373 IgG or F(ab')2 molecules led to an initial reduction in relative fluorescence intensity during the first 10-30 s after acidification compared to EEEV-373 Fab molecules or negative controls (i.e., irrelevant controls or absence of antibody) (Fig. 7E). This finding suggests bivalent EEEV-373 molecules inhibit initial fusion of SINV/EEEV particles with liposomes or delay fusion kinetics. As time progressed, however, relative fluorescence levels were comparable to those of the negative controls. The reason for this finding is not entirely known. The inability to completely abolish fusion even at saturating concentrations may occur due to incomplete occupancy of necessary epitopes on the virion to block fusion, which enables the virus to compensate for partial occupancy or EEEV-373 binding and subsequently to fuse. Alternatively, multiple mechanisms of action may be at play for the potent neutralization of SINV/EEEV observed by EEEV-373.

EEEV-373 fails to inhibit SINV/EEEV egress

Lastly, we assessed the ability of EEEV-373 to inhibit egress of SINV/EEEV from infected cells, using an established egress assay 40 . Briefly, BHK-21 cell culture monolayers were inoculated with SINV/EEEV at an MOI of 1 for 2 h at 37 °C. Cells were washed extensively to remove any unbound virus and then incubated with EEEV-373 or the negative control mAb rDENV-2D22 as IgG molecules in the presence of ammonium chloride to prevent de novo infection. Supernatant was harvested following 1 or 6 h to isolate and detect newly made viral RNA molecules by qRT-PCR. Compared with the previously published negative control 40 , EEEV-373 did not significantly inhibit SINV/EEEV egress from BHK-21 cells (Fig. 7F).

During the alphavirus replication cycle, viral intermediates displaying heterodimers of E2 and E1 are formed on the surface of infected cells prior to egress⁴⁷. Given the observed preferential binding mode of EEEV-373 as IgG molecules to SINV/EEEV particles and lack of detectable inhibition of viral egress, we hypothesized that EEEV-373 may not bind to the intermediate forms of EEEV during viral infection. To test this model, we transiently transfected cells with the structural polyprotein (capsid-E3-E2-6K-E1) of EEEV strain FL93-939 and assessed binding of EEEV-373 IgG molecules (Fig. S8). Compared to the positive

control mAb EEEV-106^{39,40}, we observed minimal binding of EEEV-373 to the EEEV structural proteins expressed on the cell surface. This observation supports the hypothesis that EEEV-373 binds to a preferred conformation present principally on intact virions.

Discussion

In this study, we present the structural and molecular basis of epitope recognition and mechanism of action of the potently neutralizing and protective anti-EEEV human mAb EEEV-373. Several aspects of this interaction are interesting from the perspective of therapeutic antibody development and structure-guided immunogen design for vaccine development. First, we present a cryo-EM structure of SINV/EEEV particles in complex with an intact IgG1 molecule. This work adds to a growing but a small list of IgG1-antigen complex structures^{8,9}. Structures of virus-antibody complexes reveal features of interactions that are not always obvious from the corresponding structures of Fab molecules. For example, the bivalent nature and flexibility of the two arms of the antibody can lead to preferred engagement of sites on the viral surface. Monovalent Fab molecules may or may not recapitulate this preferred recognition aspect of the interaction, and thus these studies may lead to inaccurate representation of Fab occupied viral epitopes. As we see in this reconstruction, EEEV-373 preferentially cross-links the two q3-spikes across the i2 axis.

The quaternary epitope revealed by the reconstruction presented here is unique in that the CDRs of EEEV-373 primarily contact residues in domain B and the β-ribbon connector of the E2 glycoprotein. The observed heavy chain CDRH2 interaction with residue K61 of the E1 glycoprotein is largely due to its long side chain, as no other surrounding E1 residues contribute to the binding footprint. This binding mode differs from that reported for the murine anti-chikungunya virus (CHIKV) mAb CHK-263 IgG, which binds to a similar area on CHIKV particles⁹. At the i2 axis, two CHK-263 IgG molecules engage the four g3 spikes. However, due to the low resolution of the reconstructions, the connectivity between the Fab arms of the two IgGs could not be ascertained. The binding modes of CHK-263 IgG suggested by authors correspond to the q3.1–q3.4 and q3.3–q3.4 alternative binding modes depicted here for EEEV-373 (Fig. 6). Like EEEV-373, weak density of CHK-263 around the i5 axis was also observed, which the authors interpreted as a flexible interaction. In contrast to EEEV-373, CHK-263 tilts ~17.5° towards and makes contacts with the E1 glycoprotein (Fig. S5). This difference in the angle of approach may be one of the reasons one EEEV-373 IgG molecule binds diagonally across the i2 axis on SINV/EEEV particles, whereas two CHK-263 IgG molecules are able to bind CHIKV particles. The heavy and light chains of CHK-263 are also flipped with respect to the corresponding chains of EEEV-373. Furthermore, CHK-263 binds as monovalent Fab molecules, which may occur due to recognition of a stabilizing quaternary epitope comprising both proteins of the E2/E1 heterodimer (as K61 and C63 of CHIKV E1 domain II also bind the CDRs of CHIK-263). The 'arch 2' cleft of the E2 protein β-ribbon connector into which the CDRH3 of EEEV-373 inserts is stabilized by the extensive interactions with the underlying E1 glycoprotein. It is this interaction that renders the epitope conformational and quaternary, which is validated by the ELISA binding data showing that bivalent EEEV-373 does not bind either recombinant monomeric E2 or E1 glycoproteins but binds to the E2/E1 heterodimer and VLPs (Fig. 2A).

The bivalency requirement for complex formation is a remarkable feature of EEEV-373. Monovalent Fab molecules of neutralizing antiviral antibodies tend to have lower affinity to viruses compared to their bivalent counterpart due to the absence of avidity effects. However, the weak detectable binding observed for monovalent EEEV-373 Fab molecules is consistent with the requirement for bivalency to neutralize EEEV. The biphasic nature of association observed in the kinetic analyses strongly supports the contribution of avidity effects towards complex formation. The dependence on avidity may stem from the

flexibility of the heterodimer epitope, necessitating slower interactions for stable complex formation. Given the lack of significant secondary structural elements in the β -ribbon connector, the 'arch 2' cleft may undergo structural transitions, leading to flexibility in the epitope. However, this could not be visualized due to the limited resolution of this region. Another explanation may result from binding of one Fab arm of the IgG molecule to the heterodimer epitope during the fast initial binding interaction step, while the other Fab arm transiently samples additional heterodimer epitopes in a slower fashion until recognizing the correct orientation to generate a high affinity complex. In such scenarios, avidity contributions from bivalent engagement of the IgG with virus particles shifts the equilibrium towards a stable complex formation.

The relatively high potency and intra-virion cross-linking displayed by EEEV-373 mirrors the activity of another potently neutralizing anti-EEEV antibody, EEEV-106⁴⁰. The ability to form intra-virion crosslinks on the icosahedral viral surface appears to correspond well with the high potency of neutralizing antibodies. The intra-virion cross-linking observed for EEEV-373 appears to be structurally constrained as the binding mode of EEEV-373 observed in the reconstruction strongly suggests that there is limited flexibility of the Fab arms with respect to one another. Theoretically, there are six possible ways the spikes across the i2 axis can be cross-linked by EEEV-373 (Fig. 6). As discussed, three of these binding modes (i3.1-q3.1, q3.1-q3.4, or q3.3-q3.4) are not feasible due to distance or steric constraints. However, while the remaining three modes (i3.1-i3.2, q3.1-q3.3, and q3.1-i3.2) satisfy both conditions, only one binding orientation was observed (q3.1-q3.3). In the i3.1-i3.2 binding mode, the Fab arms must stretch by ~50% to simultaneously bind (Fig. 6D). In the q3.1-i3.2 binding mode, IgG binding would require the Fab arms to rotate around the IgG 2-fold axis by ~60° with respect to each other (Fig. 6F). It is not obvious from the structure why these two alternative binding modes are not observed. It may be that EEEV-373 transiently interacts with these orientations prior to binding the observed preferred orientation (q3.1-q3.3). This outcome may result from an energetically favorable interaction with the q3.1-q3.3 binding mode.

EEEV-373 neutralizes EEEV by acting at multiple steps in the viral entry pathway (Fig. 7). EEEV-373 reduced ApoER2 or VLDLR binding by 80 or 50%, respectively, which suggests EEEV-373 binds near the receptor binding site or may sterically hinder the virus particles from binding to receptors (Fig. S4B). The incomplete extent of receptor blockade may be attributed to the exposure of additional epitopes besides those that are occupied by EEEV-373 IgG1 molecules. The receptor binding site for ApoER2 and VLDLR is thought to overlap on virus particles, as soluble VLDLR blocks EEEV infection of K562 cells overexpressing ApoER228. The observed differences in receptor blockade by EEEV-373 may be due to differences in binding affinity to virus particles. The apparent affinity of VLDLR to EEEV VLPs is ~2.1 to 15 nM^{29,31}, whereas EEEV-373 binds to EEEV VLPs with an affinity of ~14 nM. The strong affinity of VLDLR to EEEV VLPs may enable the receptor to outcompete EEEV-373, which may explain the incomplete blockade of VLDLR. In contrast, the affinity of ApoER2 to EEEV VLPs is not known. However, based on the results, this interaction may have lower affinity due to greater blockade of ApoER2 by EEEV-373.

Even after SINV/EEEV attachment to cells, EEEV-373 maintains neutralization activity, albeit at a -8-fold reduced potency. Post-attachment neutralization activity suggests EEEV-373 also inhibits viral entry into cells. Furthermore, bivalent EEEV-373 molecules (IgG or F(ab')2) inhibit early fusion events in the endosome, as suggested by its ability to prevent low pH-induced fusion of SINV/EEEV with liposomes. Altogether, EEEV-373 may block or partially stall steps necessary for virus entry and fusion into the cell. The cumulative inhibitory effect of EEEV-373 at multiple steps probably explains the observed potent neutralization of SINV/EEEV and 100% protective efficacy in a mouse subcutaneous challenge model of EEEV (Fig. 1). The bivalent

requirement for EEEV-373 to neutralize SINV/EEEV entry may relate to how EEEV-373 binds to virus particles. The intra-virion cross-linking of the q3 spikes across the i2 axis suggests that SINV/EEEV particles may be stabilized, such that the necessary transitional changes for virus entry and fusion are hindered. The weak association and lack of neutralization activity against SINV/EEEV as Fab molecules supports this due to the absence of avidity effects.

EEEV-373 IgG1 molecules did not block viral egress from infected cells, and the antibody minimally binds to E2 or E1 proteins expressed at the plasma membrane (Fig. S8). These findings strongly suggest that the epitope is not assembled in the proper quaternary formation or is inaccessible during virus particle assembly and egress from the plasma membrane of infected cells. The structural arrangement of glycoproteins on intact virions presents the correct geometry (i.e., distance, angle, and curvature) for EEEV-373 to engage with its epitope, which is otherwise transient or absent on the plasma membrane of transiently transfected or infected cells during budding of virus progeny.

EEEV-373 is interesting because of its recognition of a complex dynamic antigenic site. The occurrence of bivalent interactions required for stable binding and efficient neutralization allows the antibody to perform multiple functions with less molecules. Complex epitopes on viral surface antigens are attractive vaccine targets since the neutralizing antibodies that target them tend to be potent. Additionally, antibodies targeting complex conserved epitopes may provide broad protection against different serotypes or lineages of viruses. For example, for flaviviruses, such as dengue (DENV), antibodies that target quaternary epitopes within the E protein dimers show potent neutralization capability against all four DENV serotypes⁴⁸. Similarly, another potently neutralizing antibody currently in clinical development, designated ZIKV-117, neutralizes Zika virus strains from different lineages and targets a quaternary epitope spanning across E protein dimer-dimer interfaces^{49,50}. In contrast to flaviviruses like dengue, Zika and West Nile viruses, the structural characterization of quaternary epitopes on alphaviruses is lacking. Interestingly, cryo-EM reconstructions of alphaviruses in complex with protein receptors have shown the receptor binding site to interact with residues in both the E2 and E1 glycoproteins, thus, rendering alphavirus receptor binding a quaternary interaction^{24,26,29,31}. To the best of structural characterization of a knowledge, conformationally-dependent epitope on the E2 glycoprotein of a major alphaviral pathogen targeted by a patient-derived human antibody has not been previously observed. The strict dependence on bivalency for binding and neutralization displayed by EEEV-373 highlights surprising intricacies of the antigen-antibody interaction. The elucidation of this complex interaction has important implications for therapeutic antibody developments against viral pathogens. Altogether, the work described here helps inform us on the rational design of immunogens for EEEV and likely other clinically relevant alphaviruses to elicit protective responses to complex epitopes.

Methods

Human subject information

EEEV-373 was isolated from one research subject as previously described in ref. 42. Briefly, peripheral blood mononuclear cells (PBMCs) were isolated from peripheral blood samples by density gradient purification and cryopreserved until use. Written informed consent was given from the subject and protocols were approved by the Institutional Review Board (IRB) at Vanderbilt University Medical Center for the recruitment and collection of blood samples used in this study (8675).

Mouse model

Animal models were performed as previously described in refs. 40,42. C57BL/6 mice were purchased from Jackson Laboratories. All animal procedures were carried out in accordance with the recommendations

in the Guide for the Care and Use of Laboratory Animals of the National Institutes of Health. The protocols were approved by the Institutional Animal Care and Use Committee at the Utah State University IACUC protocol #10025.

Cell lines

Cell lines were maintained as previously described in refs. 39,40,42. Routine mycoplasma detection was performed using a universal mycoplasma detection kit (ATCC) and in all cases gave negative results for the cell lines tested except for the kit positive control reagent.

Viruses and virus-like particles (VLPs)

The chimeric virus Sindbis virus (SINV; TR339)/Eastern equine encephalitis virus (EEEV; strain FL93–939) was previously described in ref. 43. Briefly, the structural proteins genes of SINV TR339 were replaced with the structural protein genes of EEEV (FL93-939) under control of the SINV 26S subgenomic promoter in the cDNA clone. For wild-type virus neutralization studies, EEEV (strain FL93-939) was derived from a cDNA clone as previously described in refs. 39,51. For animal studies, the EEEV FL93-939 strain used was obtained from Dr. Robert Tesh, World Reference Center for Emerging Viruses and Arboviruses (University of Texas Medical Branch), Galveston, TX and passaged twice in Vero cells prior to use in mice^{40,42}. Purified EEEV VLPs were kindly provided by Dr. John Mascola⁵².

Recombinant proteins

Recombinant EEEV E2/E1 and monomeric E1 proteins (strain FL93-939) were expressed and purified as previously described, respectively^{39,40}. Briefly, the proteins were codon-optimized, synthesized, and cloned into the mammalian expression vector pcDNA3.1(+). Recombinant proteins were produced in Expi293F cells using the ExpiFectamine 293 transfection kit according to manufacturer's instructions (Thermo Fisher Scientific). Cell supernatant was clarified and purified through a HisTrap excel column (Cytiva) on an ÄKTA pure 25 M chromatography system. Recombinant EEEV E3E2/E2 (strain v105), which contains a mixture of E3E2 and E2 glycoproteins, was purchased from IBT Bioservices.

SINV/EEEV production and purification

For binding and neutralization assays, SINV/EEEV was produced using the methods previously described in refs. 39,42. For cryo-EM studies, SINV/EEEV was purified according to the previously described protocol^{6,40}. For liposomal fusion inhibition studies, SINV/EEEV was purified and labeled with Vybrant DiD cell-labeling solution as previously described in ref. 40.

Human hybridoma antibody generation and sequence analysis EEEV-373 hybridoma cell lines secreting EEEV-373 IgG was generated, selected, and purified as previously described in refs. 39,40,42. Recombinant mAbs were produced using the ExpiCHO expression system (Thermo Fisher Scientific) as previously described in ref. 42. Antibodies were purified from clarified supernatants using HiTrap MabSelect SuRe (Cytiva) columns on an ÄKTA Pure 25 M chromatography system and further concentrated using 50 K MWCO Amicon® Ultra centrifugal filter units (MilliporeSigma), desalted, and buffer exchanged with 7 K MWCO Zeba desalting columns (Thermo Fisher Scientific). For the generation of EEEV-373 Fab or F(ab'2) molecules, hybridoma mAb was cleaved using the IgdE cysteine enzyme FabA-LACTICA® (Genovis) as previously described in ref. 42 or using the IdeS protease (Promega), respectively. Briefly, IgG was incubated with FabALACTICA® or IdeS protease (1 unit/1 µg of IgG) overnight at room temperature or 37 °C for 30 to 60 min, respectively. Fab or F(ab'2) molecules were then purified using the CaptureSelectTM IgG-Fc affinity matrix (Thermo Fisher Scientific). For sequence analysis of EEEV-373 (Supplementary Tables 2, 3), the gene segments and V-region

nucleotide percent identity compared to germline were determined using the ImMunoGenetics (IMGT) database as previously described in refs. 39.42.

Protein EC₅₀ ELISA

To determine the binding EC₅₀ values of EEEV-373 to recombinant antigens an ELISA was performed as previously described in refs. 39,42. Briefly, EEEV VLPs (2 µg/mL) and recombinant EEEV E3E2/E2 (2 µg/mL), E2/E1 (3.84 μ g/mL), or E1 (2 μ g/mL) proteins were diluted in 1× D-PBS to coat 384-well ELISA plates (Thermo Fisher Scientific) and incubated at 4 °C overnight. The plates were aspirated and incubated with blocking solution (2% non-fat dry milk (Bio-Rad), 2% goat serum (Thermo Fisher Scientific) in 1× D-PBS-T [1× D-PBS + 0.05% Tween 20]) for 1 h at room temperature. EEEV-373 IgG, F(ab')2, or Fab molecules were initially diluted to 33 nM then serially diluted 3-fold in blocking solution (1% non-fat dry milk, 1% goat serum in 1× D-PBS-T). Abs then were added to the plates and incubated at room temperature for 2 h. The plates then were washed 3× with 1× D-PBS-T and incubated with a solution of secondary antibodies (goat anti-human kappa-HRP and goat-antihuman lambda-HRP [Southern Biotech]) diluted 1:4,000 in blocking solution (1% non-fat dry milk, 1% goat serum in 1× D-PBS-T) for 1 h at room temperature. The plates then were washed 3× with 1× D-PBS-T followed by the addition of One-StepTM Ultra-TMB ELISA substrate solution (Thermo Fisher Scientific) for ~5 min. The reaction was stopped with 1N HCl and optical density then was read at 450 nm with a BioTek[™] plate reader.

Binding kinetics analysis using a quartz crystal microbalance biosensor

EEEV VLPs (35 μg/mL) diluted in 10 mM HEPES buffer (pH 7.4) were immobilized onto LNB carboxyl sensor chips (Attana AB) by amine coupling using EDC (1-ethyl-3-[3-dimethylaminopropyl]-carbodiimide hydrochloride) and Sulfo-NHS (N-hydroxysulfosuccinimide) chemistry on the Attana CellTM 200 instrument (Attana AB). For binding assays, first to account for background binding, the sensor chips were injected with running buffer (1× HBS-T), EEEV-373 IgG (33, 8, or 0.33 nM), F(ab) 2 (35, 10, or 0.35 nM), or Fab (35, 10, or 0.35 nM) molecules diluted in running buffer then were injected to observe Ab binding to EEEV VLPs. Between Ab injections, EEEV VLP immobilized LNB carboxyl sensor chips were regenerated using 10 mM glycine pH 3.5 buffer. Assays were performed at a flow rate of 10 µL/min at 22 °C using 50- and 600 s association and dissociation times, respectively. Data were collected on the Attester software (Attana AB). A blank LNB carboxyl sensor chip was used as a reference and subtracted using the Evaluation software (Attana AB). Curves were fitted and kinetic parameters calculated using a bivalent (IgG and F(ab')2) binding model using the Trace-Drawer software (Ridgeview Instruments AB).

Binding kinetics analysis using biolayer interferometry

Biolayer interferometry was performed using an Octet® HTX system (Sartorius). Following a baseline measurement in kinetics buffer (Sartorius), $10 \,\mu\text{g/mL}$ of EEEV-373 IgG, F(ab')2, and negative control IgG molecules, or $6.7 \,\mu\text{g/mL}$ of EEEV-373 and EEEV-94 Fab molecules were separately loaded to protein L biosensors (Sartorius). The biosensors were then dipped into kinetics buffer followed by incubation with EEEV VLPs at concentrations of 0, 0.2, 0.5, 0.8, 1, or 2 nM for 300 s. Dissociation was then measured by biosensor incubation in kinetics buffer for 1800 s. A reference subtraction was performed for each antibody and curves were fitted using a 1:1 binding model. Kinetic analysis was performed using the Octet® Data Analysis v12.2 software (Sartorius).

Cell surface display EEEV binding

Binding analysis of mAbs to cells expressing alphavirus structural proteins has been previously described in refs. 39,42,53. Briefly, Expi293F cells were transiently transfected with a plasmid

(pcDNA3.1(+)) containing the structural proteins (capsid-E3-E2-6K-E1) of EEEV (strain FL93-939) using the ExpiFectamine 293 transfection kit according to manufacturer's protocols (Thermo Fisher Scientific). Cells were incubated at 37 °C in a humidified atmosphere of 8% CO $_2$ for 24 h. Cells then were harvested, fixed with 1% PFA/PBS, washed twice with 1× D-PBS, and stored at 4 °C in FACS buffer (1× D-PBS, 2% ultra-low IgG FBS, 2 mM EDTA) until use. Cells were plated at 40–50,000 cells/well in 96-well V-bottom plates. EEEV-373, rEEEV-106, or rDENV-2D22 IgG were diluted to 1 μ g/mL in FACS buffer and incubated with the cells at 4 °C for 1 h. Cells then were washed with FACS buffer and incubated with secondary antibodies (anti-human IgG-PE and anti-human IgA-PE [Southern Biotech]) diluted 1:1,000 in FACS buffer for 1 h at 4 °C. Cells then were washed in FACS buffer, and the number of events was collected on an IntelliCyt® iQue Screener Plus flow cytometer (Sartorius).

Dynamic light scattering (DLS)

DLS was performed to assess antibody-mediated aggregation of virus particles as previously described in ref. 40. Briefly, EEEV-373 IgG, F(ab') 2, or Fab molecules were mixed and incubated at 37 °C for 30 min with EEEV VLPs at Ab:VLP molar ratios ranging from 1:1 to 1,000:1. VLPs were incubated without mAb to control for particle size (-70 nm). DLS was then performed at 37 °C using a biologics stability screening platform (Uncle) and Uncle version 5.0 analysis software (Unchained Labs). Mean peak intensity was used to determine the hydrodynamic diameter (nm) of EEEV VLPs.

ApoER2 and VLDLR receptor blockade

EEEV VLPs were diluted to 2 μg/mL in 1× D-PBS to coat 384-well ELISA plates (Thermo Fisher Scientific) and incubated at 4 °C overnight. The plates were aspirated and incubated with blocking solution (2% non-fat dry milk (Bio-Rad), 2% goat serum (Thermo Fisher Scientific) in 1× D-PBS-T [1× D-PBS + 0.05% Tween 20]) for 1 h at room temperature. EEEV-373 or a negative control mAb were diluted for a final concentration of 3 to 67 nM in blocking solution (1% non-fat dry milk, 1% goat serum in 1× D-PBS-T). MAbs then were added to the plates and incubated at room temperature for 1 h. Recombinant human apolipoprotein E R2 protein (ApoER2; R&D Systems) or human very low-density lipoprotein receptor (VLDLR; R&D Systems) protein were diluted to a final concentration of 5 µg/mL. ApoER2 or VLDLR were then added to the plates and incubated at room temperature for 1h. The plates then were washed 3× with 1× D-PBS-T and incubated with a solution of secondary antibodies (anti-his-HRP [Thermo Fisher Scientific]) diluted 1:2,000 in blocking solution (1% non-fat dry milk, 1% goat serum in 1× D-PBS-T) for 1 h at room temperature. The plates then were washed 3× with 1× D-PBS-T followed by the addition of One-Step™ Ultra-TMB ELISA substrate solution (Thermo Fisher Scientific) for ~5 min. The reaction was stopped with 1 N HCl and optical density then was read at 450 nm with a BioTekTM plate reader. Percent binding of ApoER2 or VLDLR was normalized to the average optical density value for binding in the presence of the negative control mAb.

SINV/EEEV neutralization assays

Neutralization assays, including the focus reduction neutralization test (FRNT) and post-attachment assays, were formed as previously described in refs. 39,40,42. Briefly, EEEV-373 IgG, F(ab')2, or Fab molecules were initially diluted to 33 nM then serially diluted 3-fold in medium (DMEM/2% ultra-low IgG FBS/10 mM HEPES). Abs were then incubated with ~100 FFU/well of SINV/EEEV and incubated together for 1 h at 37 °C in a humidified atmosphere of 5% CO₂ or 4 °C, respectively. Virus foci were detected as previously described.

Liposomal fusion inhibition assay

Liposomes (2 mM) containing 1,2-dioleoyl-sn-glycero-3-phosphocholine (DOPC), 1,2-dioleoyl-sn-glycero-3-phosphoethanolamine (DOPE), sphingomyelin (chicken egg), and cholesterol (ovine wool) were

prepared as previously described in ref. 40. Fusion inhibition was assessed as previously described in ref. 40. Briefly, Vybrant DiD-labeled SINV/EEEV particles were incubated with EEEV-373 or negative control IgG (9 μ g), F(ab')2 (6.2 μ g), or Fab (3 μ g) molecules for 30 min at room temperature with shaking (300 rpm). Buffer with no Ab or liposome controls were also included. Prepared liposomes (2 mM) then were added, expect for the no liposome control, and loaded onto a SpectraMax iD5 multimode plate reader (Molecular Devices) at 37 °C. Sequential injections of 0.1 M MES-0.2 M acetic acid (pH 5.0) were performed using an automated injector and mixed immediately. Fluorescence (excitation at 635 nm, emission at 675 nm) then was read every 10 s for a total of 100 s.

Egress inhibition assay

Egress inhibition was performed as previously described in ref. 40. Briefly, BHK-21 cells were inoculated with SINV/EEEV (MOI 1) in medium (DMEM/2% ultra-low IgG FBS/10 mM HEPES) and then incubated at 37 °C in a humidified atmosphere of 5% CO₂ for 2 h. Cells then were washed 6× with medium containing 25 mM NH₄Cl. EEEV-373 or rDENV-2D22 IgG were diluted to 10 µg/mL in the same medium and added to the cells. The previously published negative control mAb, rDENV-2D22 IgG, and SINV/EEEV only control groups performed at the same time were included for comparison⁴⁰. The cells then were incubated at 37 °C in a humidified atmosphere of 5% CO₂ for up to 6 h. Supernatant was harvested after 1- and 6-hour incubation periods. Viral RNA then was extracted from the supernatant using the Maxwell® Viral Total Nucleic Acid purification kit on the Maxwell® system (Promega). qRT-PCR and quantification of relative RNA copies/µL were performed as previously described using the SuperScript[™] III Platinum One-Step gRT-PCR kit (Thermo Fisher Scientific)40.

SINV/EEEV escape mutant generation and analysis

To assess the ability for viral escape in the presence of EEEV-373, a realtime cell analysis (RTCA) assay and xCELLigence RTCA Multiple Plates instrument was used. The RTCA assay was performed by adding DMEM/2% ultra-low IgG FBS/10 mM HEPES to each well of a 96-well Eplate to establish a background reading. Vero cells (~18,000) were then seeded to each well of the E-plate overnight. Continuous monitoring of cell index values was performed every 15 min and analyzed using the RTCA software. Initial establishment of the neutralization potency of EEEV-373 in the RTCA assay was performed by incubating SINV/EEEV at an MOI of ~0.06 with serial three-fold dilutions of EEEV-373 or a negative control mAb starting at 10 µg/mL for 1 h at 37 °C in 5% CO₂. The virus:mAb complexes were then added to the Vero cell monolayers and continuously monitored for changes in cell index values over time. Wells containing only medium or SINV/EEEV were included as controls. Normalized cell index values approximately 48 h postinoculation were determined to establish the percent neutralization. To select for escape mutant viruses, a similar experiment was performed with some modifications. SINV/EEEV at an MOI of ~0.06 was incubated with saturating concentrations (50 and 10 µg/mL) of EEEV-373 or a negative control mAb for 1 h at 37 °C in 5% CO₂. The virus:mAb complexes were then added to the Vero cell monolayers and continuously monitored for changes in cell index values over time. Wells in which cytopathic effect was observed in the presence of EEEV-373 compared to control wells were identified as potential escape mutants and supernatant was collected.

To verify the observed phenotype, supernatants were incubated in the absence or presence of EEEV-373 (20 µg/mL), added to confluent Vero cell monolayers in a 6-well plate, and then incubated at 37 °C in 5% CO₂. Supernatants were then collected, and viral RNA was extracted using a QlAmp viral RNA extraction kit (Qiagen). cDNA corresponding to the E2 protein gene was then generated and amplified using a SuperScript™ III One-Step RT-PCR system with Platinum™ Taq DNA polymerase (Thermo Fisher Scientific) with the following forward and

reverse primers, respectively: 5' ATGTGCGTCCTGGCCAATATCAC GTTTCC 3' and 5' GAACAAAACTAGGGCAACCACTGCTGTAGC 3'. The PCR product was then purified using a QIAquick PCR purification kit (Qiagen). The resulting product was sequenced using long-read Oxford Nanopore technology (Plasmidsaurus). From the obtained sequences, variants were identified and compared to consensus sequences or the corresponding input wild-type SINV/EEEV sequence. Escape mutant viruses were identified as variants obtained only in the presence of EEEV-373.

EEEV plaque reduction neutralization test

The neutralization activity of EEEV-373 against wild-type EEEV (strain FL93-939) was performed as previously described in ref. 39. Briefly, EEEV-373 (75 nM) was serially diluted 2-fold and incubated with -100 PFU of EEEV at 37 °C for 1 h. The previously published anti-EEEV ascites fluid (ATCC) and rDENV-2D22 IgG positive and negative controls, respectively, performed at the same time were included for comparison³⁹. Ab:virus complexes then were added to Vero cell monolayer cultures and incubated at 37 °C for 1 h. An agarose overlay then was added and plates were incubated at 37 °C for 2 days. For detection of plaques, a neutral red overlay was added.

Mouse subcutaneous EEEV challenge model

Mice were challenged with EEEV by bilateral subcutaneous injections as previously described in refs. 40,42. Mice were treated with EEEV-373 at 10 mg/kg via a single intraperitoneal injection 24 h after EEEV challenge. Previously published controls, including rDENV-2D22 lgG and normal controls, performed at the same time were included for comparison 40,42. The mice were monitored for 21 days post-virus inoculation (dpi) for survival, disease signs, and body weight. Serum was collected from the mice 3 dpi to assess virus titers via an infectious cell culture assay as previously described in refs. 40,42.

Sample preparation for cryo-EM and data collection

SINV/EEEV particles were mixed with EEEV-373 at a ratio of 1:1 (virus:lgG) and 3 μL of the virus-lgG mixture was immediately loaded onto glow discharged lacey carbon grids in a BSL2-containment facility. The grids then were blotted for 3.2 s and plunge frozen in liquid ethane using a Gatan CP3. The entire process was performed under 30 s to avoid potential aggregation of the particles. The frozen grids of the complexes were imaged using a Gatan Bioquantum-K3 camera mounted on a Titan Krios (Thermo Fisher Scientific) microscope. The data collection parameters are listed in Supplementary Table 1.

Cryo-EM data processing

Data was processed as previously described in ref. 40. The resolution of the final map (4.6 Å) was calculated using the Gold Standard Fourier Shell Correlation (GSFSC) coefficient at 0.143⁵⁴. Although the quality of the map was sufficient to resolve the glycoproteins, the density of the bound IgG molecule was quite poor. To improve the density of the bound IgG, localized reconstruction of the i2 was performed. For this, sub-particles at the i2 were extracted and 3D classified into 10 classes without imposing any symmetry (C1) in Scipion⁵⁵. The best classes with well-defined structural features were pooled (289,759 sub-particles) and further refined in Relion⁵⁶ with C1 symmetry until the refinement converged. At this step, the estimated resolution according to GSFSC coefficient at 0.143 was 4.3 Å. Although the quality of the map for the bound IgG improved in comparison to the icosahedral map, it was still not useful for atomic model fitting. Therefore, a mask was applied to the two IgG bound q3 spikes and another round of 3D classification within the masked volume into three classes were carried out in Relion. One class contained with well-defined features and this class (271,460 sub-particles) was further refined using C1 symmetry in Relion. This generated a map of the bound IgG of sufficient quality to begin atomic model fitting. No density was observed for either the hinge or Fc region of the antibody. The resolution of this final map was estimated to be 3.8 Å according to the GSFSC coefficient at 0.143. Although the resolution estimation of the map is global, visual inspection revealed a resolution range across the map. Therefore, local resolution estimation of the map was carried out in Relion, which estimated the resolution of the epitope-paratope interaction surface to be around 5 Å. The map was sharpened using Autosharpen in Phenix⁵⁷. The statistics of the data collection and structure reconstruction are listed in Supplementary Table 1. A schematic of the data processing is described in Supplementary Fig. 7.

Model building and fitting into the cryo-EM density map

The ectodomain models of EEEV E2 and E1 were obtained from the Protein Data Bank (PDB ID: 6MX4). A homology model of EEEV-373 was built using AlphaFold 3. Rigid body fitting of the ectodomains and the Fab arms of the IgG into the 3.8 Å map corresponding to the two q3 spikes cross-linked by EEEV-373 were carried out in ChimeraX⁵⁸. The fitted models then were further refined against the map using the Real Space Refinement routine in Phenix⁵⁷. For the E2 and E1 ectodomains simulated annealing was included in the refinement protocol and the variable domains of the IgG were refined without simulated annealing. The resolution of the map corresponding to the constant domains were significantly worse than the rest of the map. Therefore, the constant domains were fitted as rigid bodies. The quality of the model geometry and the clash score were iteratively improved by a combination of Isolde⁵⁹, Coot⁶⁰ and real_space refinement routine in Phenix. The viral surface area buried by EEEV-373 was calculated using ChimeraX. For fitting into the icosahedral map, the refined model of one of the q3 spikes in complex with the Fab arm of the IgG and a model of the ectodomain of the i3 E2/E1 heterodimer (PDB ID: 6MX4) were fitted in UCSF ChimeraX following T = 4 quasi-symmetry of the asymmetric unit as rigid bodies. Then, the asymmetric unit around the fitted model was extracted using the phenix.map box command. Only the i3 arm of the model was subjected to the Real Space Refine routine in Phenix using default settings against the extracted map corresponding to the asymmetric unit. The model quality was improved as described above. Finally, the refined model is again fitted as a rigid body in the icosahedral map in ChimeraX following T = 4 quasi-symmetry.

Statistical analysis

All statistical analyses were performed using GraphPad Prism version 10 (GraphPad Software). Details about statistical analyses can be found in the figure legends. EC_{50} and IC_{50} values were calculated after log transformation of the concentration values and non-linear regression analysis using sigmoidal dose-response (variable slope). Survival curves were compared using the log-rank test with Bonferroni multiple comparison correction ($\rho_{adj} = 1 - (1 - \rho_{orig})^n$; n = number of comparisons).

Inclusion and ethics

The research complied with all relevant ethical regulations as established by the institutional review boards associated with all authors.

Reporting summary

Further information on research design is available in the Nature Portfolio Reporting Summary linked to this article.

Data availability

All relevant data are included within the manuscript. The source data underlying Figs. 1, 2, and 7 and Supplementary Figs. 1, 3 are provided as a Source Data file. The cryo-EM maps have been deposited in the Electron Microscopy Data Bank (EMDB) under accession codes EMD-43980 (icosahedral reconstruction of SINV/EEEV particles in complex with EEEV-373 IgG1 molecules) and EMD-43507 (localized

reconstruction map of the q3 spikes crosslinked by EEEV-373). The atomic coordinates have been deposited in the Protein Data Bank under accession codes 9AY1 (atomic model of the asymmetric unit) and 8VSV (atomic model corresponding to the localized reconstruction map). Previously published atomic models used and referred to in this study are: 6MX4 and 7CVZ. Materials described in this paper are available for distribution for nonprofit use using templated documents from Association of University Technology Managers "Toolkit MTAs", available at: https://autm.net/surveys-and-tools/agreements/material-transfer-agreements/mta-toolkit. Further information or requests for reagents may be directed to and fulfilled by the Lead Contact: Dr. Richard J. Kuhn (kuhnr@purdue.edu). Source data are provided with this paper.

References

- Crowe, J. E. Human antibodies for viral infections. Annu Rev. Immunol. 40, 349–386 (2022).
- Oliphant, T. & Diamond, M. S. The molecular basis of antibodymediated neutralization of West Nile virus. Expert Opin. Biol. Ther. 7, 885–892 (2007).
- Rey, F. A. & Lok, S.-M. Common features of enveloped viruses and implications for immunogen design for next-generation vaccines. Cell 172, 1319–1334 (2018).
- Sevvana, M. & Kuhn, R. J. Mapping the diverse structural landscape of the flavivirus antibody repertoire. *Curr. Opin. Virol.* 45, 51–64 (2020).
- Fox, J. M. et al. Broadly neutralizing alphavirus antibodies bind an epitope on E2 and inhibit entry and egress. Cell 163, 1095–1107 (2015).
- Hasan, S. S. et al. Cryo-EM structures of Eastern equine encephalitis virus reveal mechanisms of virus disassembly and antibody neutralization. Cell Rep. 25, 3136–3147.e5 (2018).
- 7. Jin, J. & Simmons, G. Antiviral functions of monoclonal antibodies against chikungunya virus. *Viruses* **11**, 305 (2019).
- Zhang, S. et al. A Human antibody neutralizes different flaviviruses by using different mechanisms. Cell Rep. 31, 107584 (2020).
- Zhou, Q. F. et al. Structural basis of Chikungunya virus inhibition by monoclonal antibodies. *Proc. Natl. Acad. Sci. USA* 117, 27637–27645 (2020).
- Armstrong, P. M. & Andreadis, T. G. Eastern equine encephalitis virus

 old enemy, new threat. N. Engl. J. Med. 368, 1670–1673 (2013).
- Ayres, J. C. & Feemster, R. F. The sequelae of Eastern equine encephalomyelitis. N. Engl. J. Med. 240, 960–962 (1949).
- 12. Lindsey, N. P., Staples, J. E. & Fischer, M. Eastern equine encephalitis virus in the United States, 2003–2016. *Am. J. Trop. Med. Hyg.* **98**, 1472–1477 (2018).
- Lindsey, N. P., Martin, S. W., Staples, J. E. & Fischer, M. Notes from the field: multistate outbreak of Eastern equine encephalitis virus — United States, 2019. MMWR Morb. Mortal. Wkly Rep. 69, 50–51 (2020).
- Ronca, S. E., Dineley, K. T. & Paessler, S. Neurological sequelae resulting from encephalitic alphavirus infection. *Front. Microbiol.* 7, 959 (2016).
- Sidwell, R. W. & Smee, D. F. Viruses of the Bunya- and Togaviridae families: potential as bioterrorism agents and means of control. *Antivir. Res.* 57, 101–111 (2003).
- Jose, J., Snyder, J. E. & Kuhn, R. J. A structural and functional perspective of alphavirus replication and assembly. *Future Microbiol.* 4, 837–856 (2009).
- Zhang, R. et al. 4.4 Å cryo-EM structure of an enveloped alphavirus Venezuelan equine encephalitis virus. EMBO J. 30, 3854–3863 (2011).
- Button, J. M., Qazi, S. A., Wang, J. C.-Y. & Mukhopadhyay, S. Revisiting an old friend: new findings in alphavirus structure and assembly. *Curr. Opin. Virol.* 45, 25–33 (2020).

- Mukhopadhyay, S. et al. Mapping the structure and function of the E1 and E2 glycoproteins in alphaviruses. Structure 14, 63–73 (2006).
- Gibbons, D. L. et al. Multistep regulation of membrane insertion of the fusion peptide of Semliki Forest virus. J. Virol. 78, 3312–3318 (2004).
- Holmes, A. C., Basore, K., Fremont, D. H. & Diamond, M. S. A molecular understanding of alphavirus entry. *PLoS Pathog.* 16, e1008876 (2020).
- Voss, J. E. et al. Glycoprotein organization of chikungunya virus particles revealed by X-ray crystallography. *Nature* 468, 709–712 (2010).
- Zhang, R. et al. Mxra8 is a receptor for multiple arthritogenic alphaviruses. Nature 557, 570–574 (2018).
- Basore, K. et al. Cryo-EM Structure of chikungunya virus in complex with the Mxra8 receptor. Cell 177, 1725–1737.e16 (2019).
- Ma, H. et al. LDLRAD3 is a receptor for Venezuelan equine encephalitis virus. Nature 588, 308–314 (2020).
- Basore, K. et al. Structure of Venezuelan equine encephalitis virus in complex with the LDLRAD3 receptor. *Nature* 598, 672–676 (2021).
- Chen, C.-L. et al. Cryo-EM structure of eastern equine encephalitis virus in complex with heparan sulfate analogues. *Proc. Natl. Acad.* Sci. USA 117, 8890–8899 (2020).
- 28. Clark, L. E. et al. VLDLR and ApoER2 are receptors for multiple alphaviruses. *Nature* **602**, 475–480 (2022).
- 29. Yang, P. et al. Structural basis for VLDLR recognition by Eastern equine encephalitis virus. *Nat. Commun.* **15**, 6548 (2024).
- Ma, H. et al. The low-density lipoprotein receptor promotes infection of multiple encephalitic alphaviruses. *Nat. Commun.* 15, 246 (2024).
- Adams, L. J. et al. Structural and functional basis of VLDLR usage by Eastern equine encephalitis virus. Cell S 0092, 01318–1 (2024).
- 32. Kielian, M. Mechanisms of virus membrane fusion proteins. *Annu. Rev. Virol.* **1**, 171–189 (2014).
- 33. Li, L., Jose, J., Xiang, Y., Kuhn, R. J. & Rossmann, M. G. Structural changes of envelope proteins during alphavirus fusion. *Nature* **468**, 705–708 (2010).
- Earnest, J. T. et al. Neutralizing antibodies against Mayaro virus require Fc effector functions for protective activity. J. Exp. Med. 216, 2282–2301 (2019).
- Jin, J. et al. Neutralizing monoclonal antibodies block chikungunya virus entry and release by targeting an epitope critical to viral pathogenesis. Cell Rep. 13, 2553–2564 (2015).
- Jin, J. et al. Neutralizing antibodies inhibit chikungunya virus budding at the plasma membrane. Cell Host Microbe 24, 417–428.e5 (2018).
- Long, F. et al. Cryo-EM structures elucidate neutralizing mechanisms of anti-chikungunya human monoclonal antibodies with therapeutic activity. Proc. Natl. Acad. Sci. USA 112, 13898–13903 (2015).
- Powell, L. A. et al. Human mAbs broadly protect against arthritogenic alphaviruses by recognizing conserved elements of the Mxra8 receptor-binding site. *Cell Host Microbe* 28, 699–711.e7 (2020).
- Williamson, L. E. et al. Human antibodies protect against aerosolized Eastern equine encephalitis virus infection. *Cell* 183, 1884–1900.e23 (2020).
- Williamson, L. E. et al. Structural constraints link differences in neutralization potency of human anti-Eastern equine encephalitis virus monoclonal antibodies. *Proc. Natl. Acad. Sci. USA* 120, e22131690120 (2023).
- Kim, A. S. et al. Pan-protective anti-alphavirus human antibodies target a conserved E1 protein epitope. Cell 184, 4414–4429.e19 (2021).

- 42. Williamson, L. E. et al. Therapeutic alphavirus cross-reactive E1 human antibodies inhibit viral egress. *Cell* **184**, 4430–4446.e22 (2021).
- Kim, A. S. et al. Protective antibodies against Eastern equine encephalitis virus bind to epitopes in domains A and B of the E2 glycoprotein. *Nat. Microbiol.* 4, 187–197 (2019).
- 44. Fibriansah, G. et al. Dengue virus. Cryo-EM structure of an antibody that neutralizes dengue virus type 2 by locking E protein dimers. *Science* **349**, 88–91 (2015).
- Sharma, A. et al. The epitope arrangement on flavivirus particles contributes to Mab C10's extraordinary neutralization breadth across Zika and dengue viruses. Cell 184, 6052–6066.e18 (2021).
- Williams, A. F. & Barclay, A. N. The immunoglobulin superfamilydomains for cell surface recognition. *Annu Rev. Immunol.* 6, 381–405 (1988).
- Chmielewski, D. et al. Chikungunya virus assembly and budding visualized in situ using cryogenic electron tomography. *Nat. Microbiol.* 7, 1270–1279 (2022).
- 48. Dejnirattisai, W. et al. A new class of highly potent, broadly neutralizing antibodies isolated from viremic patients infected with dengue virus. *Nat. Immunol.* **16**, 170–177 (2015).
- 49. Hasan, S. S. et al. A human antibody against Zika virus crosslinks the E protein to prevent infection. *Nat. Commun.* **8**, 14722 (2017).
- Sapparapu, G. et al. Neutralizing human antibodies prevent Zika virus replication and fetal disease in mice. *Nature* 540, 443–447 (2016).
- 51. Gardner, C. L. et al. Heparan sulfate binding by natural Eastern equine encephalitis viruses promotes neurovirulence. *Proc. Natl. Acad. Sci. USA* **108**, 16026–16031 (2011).
- 52. Ko, S. Y. et al. A virus-like particle vaccine prevents equine encephalitis virus infection in nonhuman primates. *Sci. Transl. Med.* **11**, eaav3113 (2019).
- 53. Kafai, N. M. et al. Neutralizing antibodies protect mice against Venezuelan equine encephalitis virus aerosol challenge. *J. Exp. Med.* **219**, e20212532 (2022).
- 54. Scheres, S. H. W. & Chen, S. Prevention of overfitting in cryo-EM structure determination. *Nat. Methods* **9**, 853–854 (2012).
- de la Rosa-Trevín, J. M. et al. Scipion: a software framework toward integration, reproducibility and validation in 3D electron microscopy. J. Struct. Biol. 195, 93–99 (2016).
- 56. Zivanov, J. et al. New tools for automated high-resolution cryo-EM structure determination in RELION-3. *Elife* **7**, e42166 (2018).
- Liebschner, D. et al. Macromolecular structure determination using X-rays, neutrons and electrons: recent developments in *Phenix*. Acta Crystallogr. D. Struct. Biol. 75, 861–877 (2019).
- 58. Pettersen, E. F. et al. UCSF ChimeraX: structure visualization for researchers, educators, and developers. *Protein Sci.* **30**, 70–82 (2021).
- 59. Croll, T. I. *ISOLDE*: a physically realistic environment for model building into low-resolution electron-density maps. *Acta Crystallogr. D. Struct. Biol.* **74**, 519–530 (2018).
- Emsley, P. & Cowtan, K. Coot: model-building tools for molecular graphics. Acta Crystallogr. D. Biol. Crystallogr. 60, 2126–2132 (2004).

Acknowledgements

We thank R. Carnahan at Vanderbilt University for helpful discussions. We thank R. Nargi, C. Gainza, J. Rodriguez, L. Handal, S. Monroig, J. Martinez, E. Villalobos, S. Seeback, J. Reidy, R. Irving, R. Troseth, and L. Myers for technical support. We thank G. DeBellis, K. Moton, T. Martin, T. Hendy, H. Darling, A. Bunnell, B. Haseltine, N. Lee, N. Suazo, and J. Mitchell for administrative assistance. We thank the Purdue cryo-EM facility for equipment access and support. L.E.W. was supported by the NIH grants T32 HL069765 and F31 Al145189. This project

received support from the NIAID grants R01 AI095366-10 (R.J.K.), U19 AI142790 (R.J.K. and J.E.C.), R01 AI172156 (J.E.C.), R01 AI41646 (W.B.K.), and the NIH/NIAID contract HHSN272201700041I, Task A51 (J.G.J.).

Author contributions

A.B. and L.E.W. contributed equally to this work. A.B. purified SINV/EEEV particles for complex formation with EEEV-373 and prepared the cryo-EM grids for data collection. A.B. and T.K. collected cryo-EM data and performed data analysis and processing. A.B. generated the reconstruction volumes, refined the atomic models, and performed the structural analyses. L.E.W. isolated, purified, and characterized EEEV-373 IgG, F(ab')2, or Fab molecules. L.E.W. performed all biochemical, biophysical, and BSL-2 neutralization assays. D.S. prepared liposomes and DiD-labeled SINV/EEEV particles, performed the fusion inhibition assay, and interpreted the results. K.B. performed the EEEV mouse studies. G.B. provided and maintained cell culture used for SINV/EEEV particle generation. A.T. analyzed viral escape mutant sequences. C.S. generated the SINV/EEEV chimeric virus. J.G.J. planned and supervised the EEEV mouse studies. T.G. performed and W.B.K. supervised the BSL-3 neutralization assays. J.E.C. and R.J.K. obtained funding and provided supervision. A.B., L.E.W., J.E.C. and R.J.K. wrote and revised the manuscript with inputs from all the authors.

Competing interests

L.E.W. has served as a consultant for BigHat Biosciences. J.E.C. has served as a consultant for Luna Labs USA, Merck Sharp & Dohme Corporation, Emergent Biosolutions, and BTG International Inc, is a former member of the Scientific Advisory Boards of Gigagen (Grifols) and Meissa Vaccines, and is founder of IDBiologics. The laboratory of J.E.C. received unrelated sponsored research agreements from AstraZeneca, Takeda Vaccines, and IDBiologics during the conduct of the study. Vanderbilt University has applied for a patent for the antibody studied in this paper. The remaining authors declare no competing interests.

Additional information

Supplementary information The online version contains supplementary material available at https://doi.org/10.1038/s41467-025-60505-x.

Correspondence and requests for materials should be addressed to James E. Crowe Jr. or Richard J. Kuhn.

Peer review information *Nature Communications* thanks Scott Pegan and the other, anonymous, reviewer(s) for their contribution to the peer review of this work. A peer review file is available.

Reprints and permissions information is available at http://www.nature.com/reprints

Publisher's note Springer Nature remains neutral with regard to jurisdictional claims in published maps and institutional affiliations.

Open Access This article is licensed under a Creative Commons Attribution-NonCommercial-NoDerivatives 4.0 International License, which permits any non-commercial use, sharing, distribution and reproduction in any medium or format, as long as you give appropriate credit to the original author(s) and the source, provide a link to the Creative Commons licence, and indicate if you modified the licensed material. You do not have permission under this licence to share adapted material derived from this article or parts of it. The images or other third party material in this article are included in the article's Creative Commons licence, unless indicated otherwise in a credit line to the material. If material is not included in the article's Creative Commons licence and your intended use is not permitted by statutory regulation or exceeds the permitted use, you will need to obtain permission directly from the copyright holder. To view a copy of this licence, visit https://creativecommons.org/licenses/by-nc-nd/4.0/.

© The Author(s) 2025